Eur. Phys. J. B **5**, 265–281 (1998)

THE EUROPEAN PHYSICAL JOURNAL B

Spatio-temporal patterns in the thermoconvection of a planar nematic layer: I. Weakly nonlinear models

E. Plaut[a,b] and R. Ribotta

Laboratoire de Physique des Solides, Université Paris-Sud, 91405 Orsay Cedex, France

Received: 1st December 1997 / Revised: 25 May 1998 / Accepted: 2 June 1998

Abstract. We study theoretically the formation of convection patterns in a laterally extended planar nematic layer heated from below, in the linear and weakly nonlinear regimes. By reformulating the viscous coupling terms of the basic nematohydrodynamic equations, a simple interpretation of the flow effects on the director dynamics can be proposed. A detailed linear analysis of the problem is presented. A *systematic method to investigate nonlinear mechanisms* is developed, and exemplified by the study of the nonlinear saturation in rolls. The extension of the roll amplitude equation with the envelope formalism is used to characterize the dynamics of the roll modulations near threshold. Coupled envelope equations are shown to describe the structure of the point defects in zig-zags observed experimentally. Finally the bifurcation to the bimodal varicose is studied. The secondary wavevector in the bimodal appears to be selected by a rotation of the director in the horizontal plane. Quantitative predictions concerning the amplitude of this rotation are given.

PACS. 47.20.Ky Nonlinearity (including bifurcation theory) – 47.20.Bp Buoyancy-driven instability – 42.70.Dr Surface-tensio-driven instability

1 Introduction

As soon as the foundations of nematohydrodynamics, the hydromechanics of nematic liquid crystals, have been posed in the early 1970s [1], convection instabilities in nematics have been intensely studied [2]. Nematics are characterized by the existence of the director field $\mathbf{n}$, the mean orientation of the elongated molecules. $\mathbf{n}$ is the direction of anisotropy of the (uniaxial) medium, and it couples to the other fields like the velocity. These properties entail a rich variety of effects and the possibility for new instabilities as compared with isotropic fluids. Therefore, new models for the study of the transition to spatio-temporal complexity in extended dynamical systems are at hand. From a theoretical point of view, because of the high order of nonlinearity of the nematohydrodynamic equations, a systematic extraction of the mechanisms which control the dynamics is challenging.

In the so-called planar geometry a layer of nematic is sandwiched between two horizontal plates where the director is fixed in a horizontal direction $\hat{\mathbf{x}}$. Since the rotational symmetry is broken new scenarios of transitions are expected. Up to now, the electroconvective instability, driven by an ac electric field, has been intensely studied, since conveniently ultra-thin layers (of thickness $d \simeq 50\ \mu$m) can be used. The characteristic times are very small ($\lesssim 1$ s), and very large aspect ratios can be reached. This "extended geometry" offers an interesting model for the study of the transition to spatio-temporal complexity in anisotropic systems, and indeed a rich phenomenology has been developed (see for instance [3] or [4]), in parallel to theoretical models which now describe a lot of features of the weakly nonlinear (WNL) regime near threshold [2]. On the contrary, the thermoconvective instability, where the basic instability mechanism (and the corresponding theory) is simpler, has only been the object of few experimental studies [5,6], and consequently of much fewer theoretical efforts. Since the primary works of Dubois-Violette [7], it is only rather recently that a systematic WNL study of this system has been performed [8]. Now, we have realized new experiments in the "director-dominated regime", at low values of the director-stabilizing magnetic fields $\mathbf{H} = H\hat{\mathbf{x}}$. These experiments have shown that, when the applied thermal gradient is increased, a cascade of structures develops (see [9] and the second part of this article [10]). It appeared therefore interesting to refine the theoretical analysis of [8], where only the first step of the cascade was modeled.

In this theoretical paper, we first introduce in Section 2 the nematohydrodynamic equations of the problem, which are highly nonlinear because of the couplings between the director field $\mathbf{n}$, the velocity field $\mathbf{v}$ and the temperature field T. A simplifying reformulation of the viscous

[a] e-mail: `plaut@theo-phy.uni-bayreuth.de`
[b] *Present address:* Physikalisches Institut der Universität Bayreuth, 95440 Bayreuth, Germany.

terms is proposed. Section 3 is devoted to a detailed three-dimensional linear analysis of the thermoconvection instability. We give approximate analytic formulae for the neutral modes, which determine to lowest order the roll structures in the WNL regime, and for the neutral surface. The selection of the critical mode is discussed, in particular in order to understand the observed experimental tendency towards oblique rolls at low magnetic fields [10]. Finally, an approximate analytical expression for the linear growth rate is given, which allows us to define semi-quantitatively the director-dominated regime. We turn in Section 4 to the study of the nonlinear properties of the system. For this purpose, we use the WNL methods treating the nonlinear terms of the equations as perturbations [11]. The eigenmodes of the linearized evolution operator of largest growth rate, the *active modes*, are used as a basis for an expansion of the solutions. After an adiabatic elimination of the *passive modes* of very negative growth rate, one is left with amplitude equations which govern the time evolution of the active modes amplitudes. It is explained here in detail how these methods can allow for a *systematic study of nonlinear mechanisms*, starting in Section 4 with the nonlinear saturation in rolls. In Section 5, the extension of amplitude equations with the envelope formalism [12] is presented, which can explain the very slow dynamics of the roll modulations near threshold observed experimentally. Section 6 presents some results for the localized zig-zag competition, and Section 7 a detailed study of the bimodal varicose secondary bifurcation of oblique rolls. We give in particular numerical predictions concerning a crucial in-plane rotation of the director. The results presented here may extend immediately to other systems of the same symmetry, whereas the methods exemplified in this paper (especially the method of investigation of nonlinear mechanisms) may be applied to any other system in the low amplitude regime.

Appendix A introduces the nematics for which we have done calculations, and recalls their material parameters. Appendix B gives the physical interpretation of the velocity potentials, and Appendix C some informations about the Galerkin method used to treat the vertical dependence of the fields.

2 Basic dimensionless equations, symmetries

2.1 Basic dimensionless equations

The director evolution equation reads in the formulation of Leslie [1]

$$\gamma_1 \mathbf{n}\times\dot{\mathbf{n}} = \mathbf{n}\times(\mathbf{h}+\mathbf{h}_v) \tag{2.1}$$

where the dot stands for the material derivative $\partial_t + \mathbf{v}\cdot\nabla$. The static molecular field $\mathbf{h}$ is the sum of elastic and magnetic terms:

$$\mathbf{h} = \mathbf{h}_d + \mathbf{h}_{magn}. \tag{2.2}$$

The elastic terms derive from the elastic free energy density f_d:

$$(\mathbf{h}_d)_i = -\frac{\partial f_d}{\partial n_i} + \partial_j \frac{\partial f_d}{\partial(\partial_j n_i)} \tag{2.3}$$

with

$$f_d = \frac{1}{2}\left[k_{11}(\nabla\cdot\mathbf{n})^2 + k_{22}(\mathbf{n}\cdot\nabla\times\mathbf{n})^2 + k_{33}(\mathbf{n}\times\nabla\times\mathbf{n})^2\right].$$

The k_{11}, k_{22}, k_{33} terms are associated with splay, twist and bend distortions of the director field respectively. For usual nematics $k_{22} < k_{11} < k_{33}$, so k_{11} is used as a scaling of the elastic constants (Tab. 1). The magnetic term is

$$\mathbf{h}_{magn} = \mu_0\chi_a(\mathbf{H}\cdot\mathbf{n})\mathbf{H}. \tag{2.4}$$

Since the magnetic susceptibility χ_a is typically positive, the director tends to align in the direction of the magnetic field. A planar magnetic field $\mathbf{H} = H\hat{\mathbf{x}}$ is therefore used in planar convection in order to increase progressively the damping of the director field. Finally, $\mathbf{h}_v$ contains all the viscous coupling terms, usually expressed in terms of the symmetric part $\underline{\underline{A}}$ and the antisymmetric part $\underline{\underline{\Omega}}$ of the gradient of velocity tensor $\underline{\underline{D}}$ ($D_{ij} = \partial v_i/\partial x_j$), as

$$\mathbf{h}_v = \gamma_1 \underline{\underline{\Omega}}\cdot\mathbf{n} - \gamma_2 \underline{\underline{A}}\cdot\mathbf{n}. \tag{2.5}$$

In (2.5) the viscosities γ_1, γ_2 are related to the viscosities α_2, α_3 by the relations

$$\gamma_1 = -\alpha_2 + \alpha_3\,,\quad \gamma_2 = \alpha_2 + \alpha_3.$$

So $\mathbf{h}_v$ can be reformulated in terms of $\underline{\underline{D}}$ only,

$$\mathbf{h}_v = -\alpha_2 \underline{\underline{D}}\cdot\mathbf{n} - \alpha_3\,\mathbf{n}\cdot\underline{\underline{D}}, \tag{2.6}$$

which separates the α_2 and α_3 contributions. As shown in Table 2 of Appendix A, for usual nematics $|\alpha_3| \ll |\alpha_2|$, so one may neglect the α_3 contribution in (2.6). This proved to only slightly influence the linear and nonlinear properties studied hereafter. Since $\alpha_2 < 0$, the coupling $\mathbf{v}\to\mathbf{n}$ can thus be approximated in planar convection by

$$\mathbf{h}_v^{simp} \simeq |\alpha_2|\ \underline{\underline{D}}\cdot\mathbf{n} = |\alpha_2|\ \lim_{\delta l\to 0}\ \frac{1}{\delta l}\Big[\mathbf{v}(\mathbf{x}+\delta l\,\mathbf{n}) - \mathbf{v}(\mathbf{x})\Big]. \tag{2.7}$$

If we suppose that the velocity field is held fixed, we see with (2.1, 2.7) that *the director tends to reorient in order to minimize* $\mathbf{n}\times(\underline{\underline{D}}\cdot\mathbf{n})$, *i.e. the director-transverse velocity gradients.*

The velocity evolution equation reads, under the assumption of incompressibility:

$$\dot{\mathbf{v}} = \rho^{-1}(\mathbf{f}_{vol} - \nabla p) + \mathbf{div}\rho^{-1}(\underline{\underline{\sigma}}^d + \underline{\underline{\sigma}}^v) \tag{2.8}$$

where ρ is the fluid density, $\mathbf{f}_{vol}$ the bulk force, p the pressure, and the divergence of the stress tensor $\underline{\underline{\sigma}} = \underline{\underline{\sigma}}^d + \underline{\underline{\sigma}}^v$ is given by [13]

$$(\mathbf{div}\underline{\underline{\sigma}})_i := \partial_j\sigma_{ij}.$$

Table 1. Definitions of the dimensionless units in terms of the basic wavevector of the vertical profiles $q = \pi/d$, where d is the thickness of the layer.

Quantity	Scaling	Interpretation of the scaling unit
elastic constant	$k_{ii} = k_{11}\ k'_{ii}$	splay elastic constant
viscosity	$\alpha_i = (\alpha_4/2)\ \alpha'_i$	isotropic viscosity
heat conductivity	$\kappa_i = \kappa_\perp\ \kappa'_i$	conductivity perpendicular to the director
length	$l = q^{-1}\ l'$	inverse wavevector of the vertical profiles
time	$t = (\kappa_\perp q^2)^{-1}\ t'$	vertical thermal diffusion time
temperature	$\theta = (\nu_a \kappa_\perp\ q^3)/(\alpha g)\ \theta'$	
magnetic field	$H = q\sqrt{k_{11}/(\mu_0 \chi_a)}\ h$	Fréederickz field $H_{\rm F}$

The elastic stress tensor $\underline{\underline{\sigma}}^d$ derives from the elastic free energy density f_d (2.3) according to

$$\sigma^d_{ij} = -\frac{\partial f_d}{\partial(\partial_j n_k)}\partial_i n_k. \tag{2.9}$$

This gives rise to terms in $(\nabla\mathbf{n})^2$ which do not intervene in the linear problem. The viscous stress tensor $\underline{\underline{\sigma}}^v$ is usually expressed as

$$\begin{aligned}\underline{\underline{\sigma}}^v = {}& \alpha_4 \underline{\underline{A}} + \alpha_1 \mathbf{n}\otimes\mathbf{n}(\mathbf{n}\cdot\underline{\underline{A}}\cdot\mathbf{n}) + \alpha_2 \mathbf{N}\otimes\mathbf{n} + \alpha_3 \mathbf{n}\otimes\mathbf{N} \\ & + \alpha_5(\mathbf{n}\cdot\underline{\underline{A}})\otimes\mathbf{n} + \alpha_6 \mathbf{n}\otimes(\mathbf{n}\cdot\underline{\underline{A}}).\end{aligned} \tag{2.10}$$

In practice in (2.10) $\underline{\underline{A}}$ has to be expanded as $\underline{\underline{A}} = \frac{1}{2}(\underline{\underline{D}} + \underline{\underline{D}}^T)$, whereas $\mathbf{N}$, the rotation of the director relatively to the fluid, has to be expanded as $\mathbf{N} = \dot{\mathbf{n}} - \underline{\underline{\Omega}}\cdot\mathbf{n}$. Thus only certain combinations of the anisotropic viscosities $\alpha_1, ..., \alpha_6$ appear in front of the components of $\underline{\underline{D}}$. In order to shorten the notations, it is convenient to introduce new viscosities

$$\begin{aligned}\gamma_3 &:= \frac{-\alpha_3 - \alpha_6}{2},\ \ \gamma_4 := \frac{\alpha_5 - \alpha_2}{2}, \\ \gamma_5 &:= \frac{-\alpha_5 - \alpha_2}{2} = \frac{\alpha_3 - \alpha_6}{2}\end{aligned} \tag{2.11}$$

with which (2.10) reduces to

$$\begin{aligned}\underline{\underline{\sigma}}^v = {}& \alpha_4 \underline{\underline{A}} + \alpha_1 \mathbf{n}\otimes\mathbf{n}(\mathbf{n}\cdot\underline{\underline{D}}\cdot\mathbf{n}) + \alpha_2 \dot{\mathbf{n}}\otimes\mathbf{n} + \alpha_3 \mathbf{n}\otimes\dot{\mathbf{n}} \\ & - \gamma_3 \mathbf{n}\otimes(\mathbf{n}\cdot\underline{\underline{D}}) + \gamma_4(\underline{\underline{D}}\cdot\mathbf{n})\otimes\mathbf{n} \\ & - \gamma_5[(\mathbf{n}\cdot\underline{\underline{D}})\otimes\mathbf{n} + \mathbf{n}\otimes(\underline{\underline{D}}\cdot\mathbf{n})].\end{aligned} \tag{2.12}$$

Note that the equivalence between the two definitions of γ_5 in (2.11) results from the Parodi relation [14]. In $\underline{\underline{\sigma}}^v$ the α_4 term gives rise to a classical $\nu_a \Delta\mathbf{v}$ term in (2.8), with $\nu_a = \alpha_4/(2\rho)$; therefore the isotropic viscosity $\alpha_4/2$ is a natural scaling of the viscosities (Tab. 1). The effective Miesowicz viscosities ν_a, ν_b, ν_c [1], defined, in the simple shear flow $\mathbf{v} = sx\hat{\mathbf{z}}$, as the ratio $\nu = \sigma^v_{zx}/(\rho s)$ for different director orientations, become simple with these notations:

(a) if the director is perpendicular to the plane of the flow, $\mathbf{n} = \hat{\mathbf{y}}$:

$$\nu = \nu_a$$

(b) if the director is parallel to the velocity field, $\mathbf{n} = \hat{\mathbf{z}}$:

$$\nu = \nu_a(1 - \gamma'_3) =: \nu_b$$

(c) if the director is in the plane of the flow, but perpendicular to the velocity field, $\mathbf{n} = \hat{\mathbf{x}}$:

$$\nu = \nu_a(1 + \gamma'_4) =: \nu_c.$$

For usual nematics the coefficients $\gamma'_3 = 2\gamma_3/\alpha_4$, $\gamma'_4 = 2\gamma_4/\alpha_4$ are positive, therefore $\nu_b < \nu_a < \nu_c$.

The heat equation reads

$$\dot{T} = \kappa_\perp\{\Delta T + \kappa'_a \nabla\cdot[(\mathbf{n}\cdot\nabla T)\mathbf{n}]\} \tag{2.13}$$

where $\kappa'_a = \kappa_\parallel/\kappa_\perp - 1$ quantifies the dimensionless anisotropy of heat diffusivity.

In order to get rid of numerous π factors in the analytic calculations, our scaling conventions are different from those of [8], but instead follow the choice made for electroconvection in [2]. With these conventions (Tab. 1), the basic wavevector of the z profiles, $q = \pi/d$, which is also the scaling of the horizontal wavevectors $\mathbf{q}$ (typically the rolls are square-like, *i.e.* of period $2d$), is now 1. The main control parameter is

$$R' = \frac{\alpha g}{\nu_a \kappa_\perp\ q^4}\ \frac{\Delta T_{app}}{d}$$

where ΔT_{app} is the difference of temperature between the lower and upper plates enclosing the nematic. The relation to the Rayleigh number R defined in [8] is:

$$R' = \pi^{-4} R. \tag{2.14}$$

The temperature field is written as the superposition of the applied gradient and a perturbation field θ: $T' = T'_0 - R'z' + \theta'$. Under the classical Boussinesq approximations, all parameters are considered as temperature independent, except the density in the bulk force $\mathbf{f}_{vol} = -\rho g\hat{\mathbf{z}}$ in (2.8): $\rho = \rho_0[1 - \alpha(T - T_0)]$, where α is the thermal-expansion coefficient of the fluid. Omitting the primes for the dimensionless quantities, we obtain

$$\begin{aligned}F\,\mathbf{n}\times\dot{\mathbf{n}} = \mathbf{n}\times\Big(&\mathbf{h}_d + h^2 n_x \hat{\mathbf{x}} + F(1+\alpha_{32})\ \underline{\underline{D}}\cdot\mathbf{n} \\ & + F\alpha_{32}\ \mathbf{n}\cdot\underline{\underline{D}}\Big)\end{aligned} \tag{2.15}$$

$$\frac{1}{Pr}\dot{\mathbf{v}} = \Delta\mathbf{v} + \theta\hat{\mathbf{z}} + \nabla p + \mathbf{div}\Big(-\frac{\alpha_2}{F}\underline{\underline{\sigma}}^d + \underline{\underline{\sigma}}^v\Big) \tag{2.16}$$

$$\dot{\theta} = \Delta\theta + R v_z + \kappa_a \nabla\cdot[(-R n_z + \mathbf{n}\cdot\nabla\theta)\mathbf{n}] \tag{2.17}$$

where in $\mathbf{h}_d$, $\underline{\underline{\sigma}}^d$, $\underline{\underline{\sigma}}^v$ the dimensionless elastic constants and viscosities must be used. We have introduced the small parameter $\alpha_{32} = \alpha_3/\alpha_2$, and

$$Pr = \frac{\text{viscous diffusivity}}{\text{thermal diffusivity}} = \frac{\nu_a}{\kappa_\perp}$$
$$F = \frac{\text{thermal diffusivity}}{\text{orientational diffusivity}} = \frac{\kappa_\perp \gamma_1}{k_{11}}. \qquad (2.18)$$

Typically these numbers are quite large; see Appendix A for some numerical values. In all equations, we eliminate n_x as $n_x = 1 - \frac{1}{2}(n_y^2 + n_z^2)$. This insures up to cubic order the normalization condition $\mathbf{n}^2 = 1$. With the use of the velocity potentials f and g (Appendix B), the local state vector of the fluid reads finally

$$V = (\theta, n_y, n_z, f, g). \qquad (2.19)$$

As long as $n_x > 0$, the director equations (2.15), which are of the form $\mathbf{n} \times \mathbf{S} = \mathbf{0}$, are equivalent to $\hat{\mathbf{z}} \cdot (\mathbf{n} \times \mathbf{S}) = 0$ and $-\hat{\mathbf{y}} \cdot (\mathbf{n} \times \mathbf{S}) = 0$, which constitute our n_y and n_z equations. The f and g equations are obtained like in [8]. The basic equations of the problem (2.15-2.17) then take the form

$$D \cdot \partial_t V = L_R \cdot V + N_2(V,V) + N_3(V,V,V) + h.o.t. \qquad (2.20)$$

where D, L_R are linear, N_2, N_3 nonlinear differential operators.

2.2 Symmetries

The translational invariance in the horizontal plane implies that the linear eigenmodes of the evolution operator are horizontal Fourier modes in which the vertical dependence of the fields can be factorized. Thus the roll modes are characterized by their horizontal wavevector $\mathbf{q} = q\hat{\mathbf{x}} + p\hat{\mathbf{y}}$, and by their vertical dependence in z. In the planar layer geometry, there is no more rotational symmetry in the horizontal plane, but the reflection S: $\hat{\mathbf{y}} \mapsto -\hat{\mathbf{y}}$ is still a global symmetry. Therefore we distinguish as usual the normal rolls (NR) $q \neq 0, p = 0$ from the oblique rolls (OR) $q \neq 0, p \neq 0$ and the parallel rolls (PR) $q = 0, p \neq 0$ [2]. S is spontaneously broken only in the OR case, where the full roll solutions of (2.20) can be split in two families, the "zigs" of wavevector such that q, $p > 0$, and the "zags" of wavevector such that $q > 0$, $p < 0$. A Fourier component of a zig roll solution can be changed into the corresponding Fourier component of a zag roll solution according to the rule

$$(\theta, n_y, n_z, f, g) \exp(i\mathbf{q} \cdot \mathbf{r}) \longrightarrow (\theta, -n_y, n_z, f, -g) \exp(iS(\mathbf{q}) \cdot \mathbf{r}). \qquad (2.21)$$

The vertical dependence of the linear eigenmodes is either of the type +, such that $\theta(z)$, $n_z(z)$, $f(z)$ are even, $n_y(z)$, $g(z)$ are odd under the reflection with respect to the midplane of the layer $z \mapsto -z$, or of the type −, such that $\theta(z)$, $n_z(z)$, $f(z)$ are odd, $n_y(z)$, $g(z)$ are even. The equations (2.20) have the important "Boussinesq-like" symmetry property

$$\text{sym}[N_2(a,b)] = -\,\text{sym}(a)\ \text{sym}(b)$$
$$\text{sym}[N_3(a,b,c)] = +\,\text{sym}(a)\ \text{sym}(b)\ \text{sym}(c) \qquad (2.22)$$

where $\text{sym}(a) = \pm 1$ according to the type of the mode a.

3 Linear properties

We apply the Galerkin method, of rapid convergence, to treat the vertical dependence of the fields (see [8] and Appendix C). The linear active modes are of the + type. They are written $V_1 = V_1(\mathbf{q}; R) + c.c.$, where $V_1(\mathbf{q}; R)$ is the Galerkin solution of

$$\sigma(\mathbf{q}; R)\ D \cdot V_1(\mathbf{q}; R) = L_R \cdot V_1(\mathbf{q}; R). \qquad (3.1)$$

With a minimal order of truncation of the Galerkin expansion, $n_{max} = 2$,

$$V_1(\mathbf{q}; R) = \Big(\ \tilde{\theta} S_1(z),\ \tilde{n}_y S_2(z),\ i\,\tilde{n}_z S_1(z),\ \tilde{f} C_1(z),\ \tilde{g} S_2(z)\Big) exp(i\mathbf{q}\cdot\mathbf{r}), \qquad (3.2)$$

and the problem (3.1) can be solved analytically for the *neutral modes* of zero growth rate $\sigma(\mathbf{q}; R) = 0$. We will deduce from this the *neutral surface* in the $(\mathbf{q}, R)$ space, defined by

$$\sigma(\mathbf{q}; R) = 0 \iff R = R_0(\mathbf{q}). \qquad (3.3)$$

In (3.2), $S_n, C_n(z)$ are basis functions which fulfill the boundary conditions (Appendix C); $\mathbf{r} = x\hat{\mathbf{x}} + y\hat{\mathbf{y}}$ is the horizontal position in the layer. We detail the calculations in order to introduce progressively all the coefficients involved and to analyze the structure of the velocity and director fields in rolls; additionally, all the linear mechanisms favoring OR at threshold (in particular at very low magnetic fields) will be discussed.

3.1 Neutral modes and neutral surface

The Galerkin Equations used for the calculations are given in Appendix C. From the g equation (C.5) one obtains that in OR ($qp \neq 0$) the flow does not stay in the $(\mathbf{q}, \hat{\mathbf{z}})$ plane, since a small $v_\parallel$ component (see Eq. (B.4)) exists:

$$\tilde{g} = qp\ \frac{(\gamma_3(\mathbf{q}^2 + 4) - \alpha_1 q^2)\ \langle C_1 | - S_2' \rangle}{\mathcal{V}_{gg}}\ \tilde{f} \qquad (3.4)$$

with

$$\mathcal{V}_{gg} = \nu_c q^4 + \nu_b p^4 + (\nu_b + \nu_c + \alpha_1) q^2 p^2 + 4(q^2 + \nu_b p^2). \qquad (3.5)$$

Solving the f equation (C.4) then shows that the temperature modulation θ drives the flow through the buoyancy force:

$$\tilde{f} = \frac{\mathbf{q}^2 \langle C_1|S_1\rangle}{\mathcal{V}_{gf}\,\mathcal{V}_{ff}}\,\tilde{\theta} \tag{3.6}$$

with

$$\mathcal{V}_{ff} = (\nu_b q^2 + p^2)\lambda_1^4 + [\mathbf{q}^2((\nu_b+\nu_c)q^2 + 2p^2) + \alpha_1 q^4] \times \langle C_1| - C_1''\rangle + \mathbf{q}^4(\nu_c q^2 + p^2), \tag{3.7}$$

$$\mathcal{V}_{gf} = 1 - (qp)^2\,\frac{(\gamma_3(\mathbf{q}^2+4) - \alpha_1 q^2)^2\,\langle C_1| - S_2'\rangle^2}{\mathcal{V}_{ff}\;\mathcal{V}_{gg}}\cdot \tag{3.8}$$

In the effective viscosities $\mathcal{V}_{gg}$ and $\mathcal{V}_{ff}$, the contributions of $\nu_a = 1$, $\nu_b = 1-\gamma_3$, and $\nu_c = 1+\gamma_4$ are mixed depending on the orientation of the wavevector $\mathbf{q}$, *i.e.* on the geometry of the corresponding flows. In equation 3.6, $\mathcal{V}_{gf} < 1$ indicates a reduction of the effective viscosity in OR due to the excursion of the flow off the $(\mathbf{q}, \hat{\mathbf{z}})$ plane (3.4), which selects a kind of optimal combinations of the viscosities ν_a, ν_b, ν_c. The elimination of n_y from the director equations (C.2, C.3) then shows that the director rotates off the (x,z) plane only in OR:

$$\tilde{n}_y = -\frac{F\,\langle S_2|C_1'\rangle}{K_{gzy}\;K_{yy}}\;qp\;\tilde{f} \tag{3.9}$$

with

$$K_{yy} = k_{33}q^2 + k_{11}p^2 + 4k_{22} + h^2, \tag{3.10}$$

$$K_{zz} = k_{33}q^2 + k_{22}p^2 + k_{11} + h^2, \tag{3.11}$$

$$K_{gzy} = \frac{1 - (k_{11}-k_{22})^2\,\langle S_2|S_1'\rangle^2\,p^2/(K_{zz}K_{yy})}{1 - q^2(\gamma_3(\mathbf{q}^2+4) - \alpha_1 q^2)/\mathcal{V}_{gg} + (k_{11}-k_{22})I_1\mathbf{q}^2/K_{zz}} \tag{3.12}$$

and $I_1 = \langle S_1|C_1\rangle\,\langle S_2|S_1'\rangle\,/\,\langle S_2|C_1'\rangle$. One also obtains that the n_z modulation results from the shear-induced orientational torque in $\partial_x v_z = iq\mathbf{q}^2 f$:

$$\tilde{n}_z = \frac{F\,\langle S_1|C_1\rangle}{K_{gyz}\,K_{yz}\,K_{zz}}\;q\mathbf{q}^2\;\tilde{f} \tag{3.13}$$

with

$$K_{yz} = \frac{1 - (k_{11}-k_{22})^2\,\langle S_2|S_1'\rangle^2\,p^2/(K_{zz}K_{yy})}{1 + (k_{11}-k_{22})I_2 p^2/(\mathbf{q}^2 K_{yy})}, \tag{3.14}$$

$$K_{gyz} = 1 + \frac{(k_{11}-k_{22})\;I_2 q^2 p^2(\gamma_3(\mathbf{q}^2+4) - \alpha_1 q^2)}{\mathcal{V}_{gg}K_{yy}\;\mathbf{q}^2}, \tag{3.15}$$

and $I_2 = \langle S_2|S_1'\rangle\,\langle S_2|C_1'\rangle\,/\,\langle S_1|C_1\rangle$. The factor K_{yz}, smaller than 1 as soon as $p \neq 0$, appears as a lowering of the effective elastic constant K_{zz} in (3.13) due to the director rotation (3.9). The factor K_{gyz}, slightly larger than 1 when $p \neq 0$, expresses an increase of the effective elastic constant K_{zz} resulting from the couplings $g \to n_y \to n_z$. This effect is nevertheless generally overcomed by the previous one, since we observe the hierarchy $1 - K_{yz} \gg K_{gyz} - 1 > 0$. Finally, the value of $R = R_0(\mathbf{q};h)$ follows from the heat equation (C.6) expressing the balance between the heat-diffusion damping, characterized by an effective heat-diffusivity

$$\mathcal{K} = (1+\kappa_a)\;q^2 + p^2 + 1 = \kappa_\parallel q^2 + p^2 + 1, \tag{3.16}$$

and the enhancement of heat modulations by the convective transport (term $Rv_z = R\mathbf{q}^2 f$) and by the heat focusing (term $-R\kappa_a\partial_x n_z$). The splitting of $R_0(\mathbf{q};h)$ into a isotropic and anisotropic factors, found in [5] within a simplified one-dimensional model, still holds within our three-dimensional model [15]:

$$R_0(\mathbf{q};h) = R_0^{iso}(\mathbf{q})\;Foc(\mathbf{q};h) \tag{3.17}$$

where

$$R_0^{iso}(\mathbf{q}) = \frac{\mathcal{K}\,\mathcal{V}_{gf}\,\mathcal{V}_{ff}}{\mathbf{q}^4\,\langle S_1|C_1\rangle^2} \tag{3.18}$$

expresses the isotropic heat-convection mechanism, and the "focusing factor"

$$Foc(\mathbf{q};h) = \left(1 + \frac{F\kappa_a q^2}{K_{gyz}\,K_{yz}\,K_{zz}}\right)^{-1} \tag{3.19}$$

expresses the anisotropic convection mechanism. Because of the factor q^2 in the denominator of $Foc(\mathbf{q};h)$, this focusing occurs only for rolls with $q \neq 0$, *i.e.* with a "normal component".

3.2 Selection of the critical mode

All the effects controlling the selection of the *critical wavevector* $\mathbf{q}_c(h)$, which yields the minimum $R_c(h)$ of $R_0(\mathbf{q};h)$, can be extracted from the formula (3.17).

In the *high magnetic field limit*, one finds critical PR. Indeed, since K_{yy} and $K_{zz} \longrightarrow \infty$, the director field is frozen ($n_y = n_z = 0$): $Foc(\mathbf{q};h) = 1$ and $R_0(\mathbf{q};h)$ reduces to $R_0^{iso}(\mathbf{q})$. The instability mechanism is then the same as the isotropic thermoconvection mechanism, for which one does obtain to lowest Galerkin order the same expression as (3.18) for the neutral surface, but of course with $\kappa_\parallel = 1$ in $\mathcal{K}$, and $\gamma_5 = \nu_b - 1 = \nu_c - 1 = \alpha_1 = 0$ in $\mathcal{V}_{gf}$ and $\mathcal{V}_{ff}$. Here the remaining anisotropic effects favor PR:

(E1) the $\mathbf{q}-$dependence of $\mathcal{K}$ equation (3.16) indicates (since $1 < \kappa_\parallel$) that the temperature modulation in PR, therefore perpendicularly to the director, is less damped than in NR;

(E2) the $\mathbf{q}-$dependence of $\mathcal{V}_{ff}$ equation (3.7) indicates (since $\nu_b \simeq \nu_a = 1 \ll \nu_c$) that the viscous damping in PR is weaker than in NR. Indeed in PR the flow is in geometry a, whereas in NR the flow is in geometry c close to the mid-plane of the layer.

Therefore one obtains as for isotropic thermoconvection [16]:

$$R_c(h=\infty) = R_c^{iso} = 17.74,$$
$$\mathbf{q}_c(h=\infty) = q_c^{iso}\,\hat{\mathbf{y}} = 0.9860\,\hat{\mathbf{y}}. \tag{3.20}$$

The increase of the "isotropic" threshold for the NR case can be estimated by computing

$$\frac{R_0^{iso}(q_c^{iso}\,\hat{\mathbf{x}})}{R_c^{iso}} = (1+0.49\kappa_a)\,(1+0.25\gamma_4-0.75\gamma_3+0.14\alpha_1)$$

which shows clearly the role of the anisotropic heat diffusivities and viscosities.

In the case of *intermediate magnetic fields*, typically $10 \lesssim h \lesssim 20$, one finds critical NR. In effect, the $\mathbf{q}-$dependence in the director damping constants K_{yy} and K_{zz}, due to the orientational elasticity, is then totally overcomed by the magnetic torque: $K_{yy} \simeq K_{zz} \simeq h^2$. Consequently $K_{gyz} \simeq K_{yz} \simeq 1$ up to terms of order h^{-2}, and

$$Foc(\mathbf{q};h) \simeq \left(1+\frac{F\kappa_a q^2}{h^2}\right)^{-1}.$$

The threshold of NR is strongly reduced by this factor, since $F \simeq 800$. Indeed in NR the shear-inducing of the director modulation (term $\partial_x v_z$ in the n_z equation) and the heat-focusing (term $R\kappa_a\partial_x n_z$ in the heat equation) are in this regime more efficient (*cf.* $\partial_x \propto q$). Between these NR at intermediate magnetic fields and the PR at high magnetic fields, a continuous evolution of $\mathbf{q}_c$ occurs, with critical OR between the *Lifshitz points* h_{L1} and h_{L2}. This scenario has been first predicted (but only partially explained) in [8]. It has been confirmed experimentally in [6] with the nematic liquid crystal 5CB.

At *low magnetic fields*, a tendency towards OR exists. Indeed, the wavevector dependence of the effective elastic constants is no more suppressed by the magnetic torque, and the anisotropy of orientational elasticity comes into play, which favors OR:

(E3) the $\mathbf{q}-$dependence of K_{zz} equation (3.11) indicates (since $k_{22} < k_{33}$) a relief of bend by twist in the n_z distortion in OR;

(E4) the lowering of the effective elastic constant on n_z by the factor $K_{yz} < 1$ equation (3.14) indicates (since $K_{yz} - 1 \propto (k_{22} - k_{11}) < 0$) an indirect relaxation of splay by twist, through the introduction of a n_y distortion.

Of course these effects combine with the effects responsible for the transition towards OR at high magnetic fields, *i.e.* the effects (E1), (E2) and

(E5) the lowering of the effective viscosity on f by the factor $\mathcal{V}_{gf} < 1$ equation (3.8) indicates (since $\mathcal{V}_{gf} - 1 \propto -\gamma_3^2$) a reduction of the viscous damping in OR by the introduction of the "anomalous" (parallel to the axis of the rolls) velocity component (3.4).

For 5CB and MBBA critical NR are still found at low h, but the anisotropic effects (E1–E5) favoring OR lead to a very small curvature of the reduced threshold surface

$$\epsilon_0(\mathbf{q}) := \frac{R_0(\mathbf{q})}{R_c} - 1 \tag{3.21}$$

in the y direction. This can be demonstrated by comparing the coherence lengths ξ_{xx} and ξ_{yy} such that

$$\epsilon_0(\mathbf{q}_c + Q\hat{\mathbf{x}} + P\hat{\mathbf{y}}) \simeq \xi_{xx}^2 Q^2 + \xi_{yy}^2 P^2 \tag{3.22}$$

for small Q and P. For 5CB for instance one finds $\xi_{xx} = 1.59 \gg \xi_{yy} = 0.46$ at $h = 0$, and we will see in Section 5 that this flatness implies a very slow dynamics of the zig-zag modulations.

The effects (E1–E5) become more important if the mean temperature of the nematic material is decreased, since then $k_{33}/k_{22}, k_{11}-k_{22}, \kappa_\parallel, \nu_c$ and γ_3^2 usually increase. Thus, for a "very anisotropic" nematic material at low temperature these anisotropic effects might favor OR at threshold. Indeed, with some reasonable parameters for N4 at 20 °C, one finds a Lifshitz point h_{L0} OR $\to$ NR at very low h: $h_{L0} = 0.5$ with the full parameters of Table 3 of Appendix A; $h_{L0} = 0.8$ if we assume $\alpha_{32} = 0$ and use our analytic formula for $R_0(\mathbf{q};h)$. However, the tendency towards OR is weak, since the reduced NR threshold is only slightly positive: $\epsilon_0(|\mathbf{q}_c|\hat{\mathbf{x}}) \simeq 3\times10^{-4}$ at $h = 0$. Thus the surface $\epsilon_0(\mathbf{q})$ remains very flat in the y direction, and this explains why a very small change in the parameters (like setting $\alpha_{32} = 0$ instead of -0.023) drastically modifies the position of $\mathbf{q}_c$, even if the values of $R_0(\mathbf{q};h)$ are only slightly modified (by less than 1%). In other words, we are still close to the Lifshitz point at $h = 0$ (indeed, $\arg\mathbf{q}_c = 10°$ with the full N4 parameters, 16° if we set $\alpha_{32} = 0$) and therefore this OR selection might be difficult to evidence experimentally (see the discussion of Sect. 5). The evidence for a Lifshitz point at very low h would definitely be clearer with a nematic even more anisotropic than N4, but we do not know such a nematic for which reliable measurements of the parameters are available.

Nevertheless, we note that each of the effects enumerated above is important to explain the slight preference for OR in N4 (in [8], only the effects (E1) and (E3) were evoked). Indeed, if any of these effects is suppressed, by dropping the corresponding anisotropic terms in the linear equations, the OR domain vanishes.

Finally, the viscosity α_1, which is difficult to measure experimentally (it is know only for MBBA and 5CB), plays also a role in the selection of $\mathbf{q}_c$. Usually α_1 is negative and the main consequence is a decrease of the effective viscosity for NR because of the term $\alpha_1 q^4$ in $\mathcal{V}_{ff}$ (Eq. (3.7)). Large negative value of α_1 favors therefore NR: if one assumes *e.g.* $\alpha_1 = -0.11$ instead of 0 for N4, the OR domain at low h vanishes.

3.3 Linear dynamics

The growth rate $\sigma(\mathbf{q}_c;R)$ of the critical mode can be expanded, for small values of the reduced control parameter $\epsilon = R/R_c - 1$, as $\sigma(\mathbf{q}_c;R) \simeq \epsilon/\tau$ where τ is the characteristic time of the instability. An analytical approximate expression for τ can be found in the low-magnetic field regime within the lowest-order Galerkin expansion. Then, in the usual NR case, $n_y = g = 0$, and only the linear equations (C.3) for n_z, (C.6) for θ, and (C.4) for

f have to be solved for σ. The hierarchy of their damping constants, $K_{zz}/F \ll \mathcal{K} \ll Pr\mathcal{V}_{ff}$, indicates that we are at low magnetic fields in a "director-dominated regime" (DDR): the director is by far the weakest damped field. Thus an adiabatic elimination of the temperature and velocity fields is possible: $\sigma\tilde{\theta}$ and $\sigma\tilde{f}$ can be neglected in Equations (C.6, C.4) respectively (however one must keep the term $\propto \alpha_2\sigma\tilde{n}_z$ in the l.h.s. of the f Eq. (C.4)). This leads to

$$\tau \simeq \tau^d := \frac{F}{K_{zz}}\left[1 - Foc(\mathbf{q}_c;h) - \gamma_1\frac{q_c^2\,\mathcal{K}}{R_0^{iso}(\mathbf{q}_c)}\right] \quad (3.23)$$

where K_{zz} and $\mathcal{K}$ are taken at $\mathbf{q} = \mathbf{q}_c$. The relative distance $\delta\tau = |\tau - \tau^d|/\tau$ between this renormalized director relaxation time τ^d and the exact characteristic time τ can be considered as a quantitative test of the DDR. Indeed $\delta\tau$ is very small at small h: *e.g.* for 5CB, $\delta\tau < 0.01$ for $0 \le h \le 5$. This indicates that here, the temperature and velocity fields can indeed be treated adiabatically, and that one is in the DDR. For N4, $\delta\tau$ also stays smaller than 0.01 for $0 \le h \le 5$, even in the OR regime: the criterion $\delta\tau \ll 1$ to characterize the DDR seems to be general. It was used experimentally in [9] since it is much simpler to measure the characteristic time of the instability than the relative amplitudes $\tilde{n}_z/\tilde{\theta}$ or $\tilde{n}_z/\tilde{f}$, which should be very large in the DDR. Of course, when h increases, $\tilde{n}_z/\tilde{\theta}$ and $\tilde{n}_z/\tilde{f}$ decrease, whereas $\delta\tau$ increases, indicating that at higher h one is no more in the DDR. For instance, for 5CB, $\delta\tau \simeq 0.05$ at $h = 10$, and $\delta\tau \simeq 0.15$ at $h = 15$ [1].

We will need a general expansion of the growth rate $\sigma(\mathbf{q};\epsilon)$ of the active roll-modes. It is expressed as

$$\sigma(\mathbf{q};\epsilon) \simeq \frac{\epsilon - \epsilon_0(\mathbf{q})}{\tau_{\mathbf{q}}} \quad (3.24)$$

where $\tau_{\mathbf{q}}$ is a wavevector-dependent characteristic time, such that $\tau_{\mathbf{q}_c} = \tau$. This expansion gives σ values exact to 1% for $-0.1 \le \epsilon \le 0.5$ in a very large wavevector domain defined by $|q - q_c| < 0.5, |p| < 0.8$, which contains all the active mode wavevectors (see Fig. 5a).

4 Nonlinear roll solutions

In this section we present the first systematic study of the nonlinear saturation in rolls, based on the WNL scheme introduced for instance in [2,8,11]. For this purpose, precise definitions of the tools and the modes intervening in the amplitude equation for rolls are first set.

4.1 Amplitude equation for rolls

In order to obtain amplitude equations where the nonlinear coefficients do not depend of ϵ, we use modes at fixed R, here the neutral modes $V_1(\mathbf{q}) := V_1(\mathbf{q}; R_0(\mathbf{q}))$, instead of the full eigenmodes. The starting point of the method is to insert a roll ansatz in the basic equations:

$$V = A\; V_1(\mathbf{q}) + \overline{A}\; V_1(-\mathbf{q}) + V_2, \quad (4.1)$$

and to adiabatically eliminate the second harmonics:

$$V_2 = |A|^2\, V_2(\mathbf{q},-\mathbf{q}) + [A^2\, V_2(\mathbf{q},\mathbf{q}) + c.c.] \quad (4.2)$$

where we distinguish the homogeneous second harmonics

$$\begin{aligned} V_2(\mathbf{q},-\mathbf{q}) &= -L_{R_c}^{-1}\cdot N_2\Big(V_1(\mathbf{q})|V_1(-\mathbf{q})\Big) \\ &= \Big(\;\tilde{\theta}^H S_2(z),\;\tilde{n}_y^H S_1(z),\;0,\;0,\;0\Big) \end{aligned} \quad (4.3)$$

from the inhomogeneous second harmonics

$$\begin{aligned} V_2(\mathbf{q},\mathbf{q}) &= -L_{R_c}^{-1}\cdot N_2\Big(V_1(\mathbf{q}), V_1(\mathbf{q})\Big) \\ &= \Big(\;\tilde{\theta}^I S_2(z),\;\tilde{n}_y^I S_1(z),\;\tilde{n}_z^I S_2(z), \\ &\qquad \tilde{f}^I C_2(z),\;\tilde{g}^I S_1(z)\Big)\exp(2i\mathbf{q}\cdot\mathbf{r}). \end{aligned} \quad (4.4)$$

These modes are, according to the rule (2.22), of opposite $z-$symmetry than the linear roll modes (3.2); from now on we only write the leading Galerkin modes in the state vectors like (4.3, 4.4). The notations

$$\begin{aligned} N_2(a|b) &= N_2(a,b) + N_2(b,a) \\ N_3(a|a|b) &= N_3(a,a,b) + N_3(a,b,a) + N_3(b,a,a) \\ N_3(a|b|c) &= N_3(a,b,c) + N_3(a,c,b) + N_3(b,a,c) \\ &\quad + N_3(c,a,b) + N_3(b,c,a) + N_3(c,b,a) \end{aligned} \quad (4.5)$$

are also used.

The next step of the method requires a scalar product in V space (using the z-functional product (C.1)):

$$\begin{aligned} &\langle U(z)\exp(i\mathbf{q}\cdot\mathbf{r}), T(z)\exp(i\mathbf{q}'\cdot\mathbf{r})\rangle \\ &= \delta(\mathbf{q}-\mathbf{q}')\Big(\langle\overline{U}_\theta|T_\theta\rangle + \langle\overline{U}_{n_y}|T_{n_y}\rangle \\ &\quad + \langle\overline{U}_{n_z}|T_{n_z}\rangle + \langle\overline{U}_f|T_f\rangle + \langle\overline{U}_g|T_g\rangle\Big) \end{aligned} \quad (4.6)$$

the definition of the adjoint linear operator $L_R^\dagger$, by $\langle U, L\cdot V\rangle = \langle L^\dagger\cdot U, V\rangle$, and of the adjoint neutral modes, the solutions of

$$L_{R_0(\mathbf{q})}^\dagger\cdot U_1(\mathbf{q}) = 0$$

normalized such that

$$\langle U_1(\mathbf{q}), D\cdot V_1(\mathbf{q}')\rangle = \delta(\mathbf{q}-\mathbf{q}').$$

The projection of (2.20) on $U_1(\mathbf{q})$ gives then to lowest order

$$\partial_t A = \sigma(\mathbf{q};R)A - g_{\mathbf{q}}\;|A|^2\;A. \quad (4.7)$$

[1] When $h \to \infty$, one enters in fact a "temperature-dominated regime" since τ^d becomes smaller than $\tau^{therm} = 1/\mathcal{K} = 1/((q_c^{iso})^2 + 1) = 0.51$, which gives the asymptotic value of τ when $h \to \infty$.

There, the growth rate is defined by $\sigma(\mathbf{q};R) = \langle U_1(\mathbf{q}), L_R \cdot V_1(\mathbf{q})\rangle$, which yields at small ϵ the same values as in (3.1), and the saturation coefficient $g_{\mathbf{q}}$ reads

$$\begin{aligned} g_{\mathbf{q}} = & -\langle U_1(\mathbf{q}), T_{\mathbf{q}}\rangle \\ \text{where } T_{\mathbf{q}} = & N_2(V_1(\mathbf{q})|V_2(\mathbf{q},-\mathbf{q})) \\ & + N_2(V_1(-\mathbf{q})|V_2(\mathbf{q},\mathbf{q})) \\ & + N_3(V_1(\mathbf{q})|V_1(\mathbf{q})|V_1(-\mathbf{q})). \end{aligned} \tag{4.8}$$

A physical normalization of the roll modes in the supercritical case $g_{\mathbf{q}} > 0$ is such that one finally obtains $A = \sqrt{\epsilon - \epsilon_0(\mathbf{q})}$ when the growth rate is given by (3.24). It is:

$$U_1'(\mathbf{q}) = \sqrt{\tau_{\mathbf{q}}\, g_{\mathbf{q}}}\; U_1(\mathbf{q}), \quad V_1'(\mathbf{q}) = \frac{1}{\sqrt{\tau_{\mathbf{q}}\, g_{\mathbf{q}}}}\; V_1(\mathbf{q}). \tag{4.9}$$

Changing to these new roll modes, or equivalently defining a new amplitude according to $A' = \sqrt{\tau_{\mathbf{q}}\, g_{\mathbf{q}}} A$ (and omitting the primes), yields now:

$$\tau_{\mathbf{q}} \partial_t A = (\epsilon - \epsilon_0(\mathbf{q}))\; A - |A|^2\; A. \tag{4.10}$$

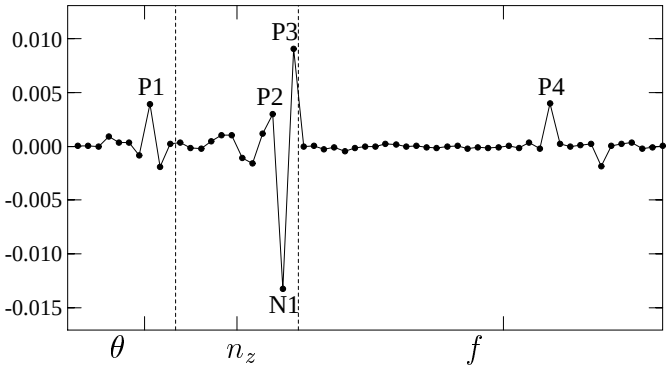

Fig. 1. Diagram of the 58 nontrivial contributions to the saturation coefficient $g_{\mathbf{q}} = +0.0041$ for normal rolls at $h = 0$ and the nematic 5CB. The first range of indices, on the horizontal axis, pertains to the contributions due to T_θ in equations (4.8, 4.6) the second range to the contributions due to T_{n_z}, and the third to the contributions due to T_f (for normal rolls $T_{n_y} = T_g = 0$). Inside each range, the ticks indicate the separation between the contributions of the quadratic and cubic terms (see *e.g.* Eq. (4.11)). The most important saturating (anti-saturating) contributions are indicated with the labels P1 to P4 (N1).

4.2 Study of the nonlinear saturation

The saturation coefficient $g_{\mathbf{q}}$ takes, like every coefficients of a WNL amplitude equation, the form of a sum equations (4.8, 4.6). Thus the contribution of each nonlinear term in the basic equations (2.20) and of each nonlinear coupling in $T_{\mathbf{q}}$ is explicitly known. For instance, labeling all the quadratic and cubic terms in the heat equation with the indices k and l, the contribution $\langle \overline{U}_\theta | T_\theta \rangle$ from the heat equation to $g_{\mathbf{q}}$ can be split as

$$\begin{aligned} T_\theta = & \sum_k \Big(N_{2\theta k}(V_1(\mathbf{q})|V_2(\mathbf{q},-\mathbf{q})) + N_{2\theta k}(V_1(-\mathbf{q})|V_2(\mathbf{q},\mathbf{q})) \Big) \\ & + \sum_l N_{3\theta l}(V_1(\mathbf{q})|V_1(\mathbf{q})|V_1(-\mathbf{q})). \end{aligned} \tag{4.11}$$

Plotting these contributions *versus* the indices will yield a diagram such that the sum of all contributions is equal to $g_{\mathbf{q}}$, and the relative importance of each contribution can immediately be judged. In order to reduce the length of the diagrams, contributions that cancel for symmetry reasons are not to be plotted [17].

If one performs this analysis on the saturation coefficient of the PR at very high h, where the convection mechanism is the isotropic one, the problem is greatly simplified since the director field plays no role ($n_y = n_z = 0$ in PR) and there is no vertical vorticity ($g = 0$). Only 7 nonlinearities in T contribute to $g_{\mathbf{q}}$ and a very simple diagram is obtained, in which a sharp peak dominates all the other contributions by at least a factor of 10. This peak is the contribution of $N_{2\theta}(V_1(\mathbf{q}), V_2(\mathbf{q},-\mathbf{q}))$ coming from the advection term $-v_z \partial_z \theta$. Since the temperature field in the homogeneous second harmonics $V_2(\mathbf{q},-\mathbf{q})$ (Eq. (4.3)) is also generated by advection terms (now $-(v_x\partial_x + v_z\partial_z)\theta$ coupling $V_1(\mathbf{q})$ and $V_1(-\mathbf{q})$), the saturation in isotropic thermoconvection is therefore a two-step procedure entirely controlled by the heat advection (additional effects may come into play at small Prandtl number, but here we assume $Pr \gtrsim 400$). An interpretation of this mechanism is that advection tends to homogenize all fields, and so always participate in the saturation of a pattern-forming instability. But this saturation by the heat advection is weak. This, together with the fact that the characteristic time is small, implies that the physically normalized roll modes (4.9) in this regime show large temperature and velocity modulations:

$$\begin{aligned} & V_1(q_c^{iso}\hat{\mathbf{y}}; h=\infty) \\ & = \underset{\theta}{\Big(} \underset{}{15\; S_1(z),} \;\; \underset{n_y}{0,} \;\; \underset{n_z}{0,} \;\; \underset{f}{1.7\; C_1(z),} \;\; \underset{g}{0} \underset{}{\Big)} \; \exp(iq_c^{iso} y) \end{aligned} \tag{4.12}$$

where in the lower row the fields in the state vector V have been recalled (see Eq. (2.19)).

On the contrary, at $h = 0$ the saturation is much stronger: $g_{\mathbf{q}}$ increases by a factor 430 between $h = \infty$ and $h = 0$ for 5CB, chosen hereafter as a typical nematic. In order to understand this change, we constructed the diagram for $g_{\mathbf{q}_c}$ at $h = 0$ in Figure 1. It contains now 58 contributions since $n_z \neq 0$ in NR. This large number is generic: nonlinear nematohydrodynamics implies the interaction of a large number of modes *via* a large number of coupling terms, and therefore in general not only one but several different nonlinear mechanisms control the value of a nonlinear coefficient. Here the more important saturating terms, which appear to impose the positive value of $g_{\mathbf{q}}$, can be distinguished as follows (labels in Fig. 1):

(P1) the contribution of $N_{3\theta}(V_1(\mathbf{q})|V_1(\mathbf{q})|V_1(-\mathbf{q}))$ due to

$\frac{1}{2}R\kappa_a\partial_x n_z^3$. This term is a correction to the heat-focusing term $-\kappa_a R\partial_x n_z$. It indicates a simple geometrical effect of diminution of the heat-focusing when the director becomes vertical;

(P2) the contribution of $N_{3n_z}(V_1(\mathbf{q})|V_1(\mathbf{q})|V_1(-\mathbf{q}))$ due to $\frac{1}{2}(2k_{33}-k_{11})n_z^2(\partial_z^2 n_z)$. It corresponds to a nonlinear elastic damping of the n_z distortion in rolls;

(P3) the contribution of $N_{3n_z}(V_1(\mathbf{q})|V_1(\mathbf{q})|V_1(-\mathbf{q}))$ due to $-F(\partial_x v_z)n_z^2$. This α_2 term is a correction to the shear term $\partial_x v_z$ in the n_z equation. It indicates that if the director rotates, the director-transverse shear, *i.e.* the excitation of the n_z distortion by the flow, is diminished;

(P4) the contribution of $N_{3f}(V_1(\mathbf{q})|V_1(\mathbf{q})|V_1(-\mathbf{q}))$ due to the source term $(\alpha_1+\gamma_3+\gamma_4)\partial_z[(\partial_z v_x)n_z^2]$ in the evolution equation for v_x. This indicates an increase of the effective viscosity for the horizontal flows in the rolls, since, as soon as the director is raised, one leaves the lowest viscosity geometry b for these flows.

In the negative, anti-saturating terms, a very dominant contribution can be identified (Fig. 1):

(N1) the contribution of $N_{3n_z}(V_1(\mathbf{q})|V_1(\mathbf{q})|V_1(-\mathbf{q}))$ due to $-F(\partial_z v_x)n_z^2$. This α_2 term indicates that when the director is raised, it becomes sensitive to the horizontal flows, which orient the director in the same direction as do the vertical flows at linear order.

The balance between all these effects can only be computed numerically, but the common feature between them is that they have a *geometrical origin*: they are due to nonlinearities generated either by the insertion of the director-normalization condition $n_x = 1-\frac{1}{2}(n_y^2+n_z^2)$ in the equations, or by the expansion of $\underline{\underline{D}}\cdot\mathbf{n}$ in (2.15). This geometrical origin implies that these mechanisms are very efficient; for instance for (P1) it is clear that if the director is completely raised ($n_z = 1$) no more heat focusing can occur! Consequently, $g_{\mathbf{q}}$ is large at $h = 0$, and this fact, together with the linear properties specific to the DDR (large characteristic times – relative scales of the fields in the linear modes: $\tilde{\theta}, \tilde{f} \ll \tilde{n}_z$), makes possible that convection develops with temperature and velocity modulations approximately 500 times smaller than in the isotropic case: now the physically normalized critical roll-mode is

$$V_1(q_c\hat{\mathbf{x}}; h=0) = \Big(\underset{\theta}{0.030\ S_1(z)},\ \underset{n_y}{0},\ \underset{n_z}{0.91i\ S_1(z)},\ \underset{f}{0.0029\ C_1(z)},\ \underset{g}{0}\Big)\ \exp(iq_c x) \tag{4.13}$$

to be compared with (4.12). As we shall see in Section 2.2, this restricts the available experimental methods for the characterization of the convective structures, where strong modulations are only obtained in the n_z field:

$$n_z = -Z_1(\mathbf{q})\ \sqrt{\epsilon-\epsilon_0(\mathbf{q})}\ \sin(\mathbf{q}\cdot\mathbf{r})\ S_1(z) + h.o.t.$$
$$\text{with}\quad Z_1(\mathbf{q}) = 2\tilde{n}_z' = \frac{2}{\sqrt{\tau_{\mathbf{q}}\ g_{\mathbf{q}}}} \tag{4.14}$$

according to equations (4.1, 3.2, 4.9, 4.10) (assuming a pre-normalization of $V_1(\mathbf{q})$ such that $\tilde{n}_z = 1$). In fact, experimentally the wavevector $\mathbf{q}$ of the rolls changes with increasing ϵ, moving progressively from $q_c\hat{\mathbf{x}}$ at threshold to $\mathbf{q}_f = q_{\rm f}\ \hat{\mathbf{x}} + p_{\rm f}\ \hat{\mathbf{y}} = q_c(1.06\hat{\mathbf{x}} + 0.15\hat{\mathbf{y}})$ (Eq. (4.3) of [10]) before the bimodal instability. The n_z amplitude $Z_1(\mathbf{q})$ (Eq. (4.14)) should then evolve accordingly. During this evolution of $\mathbf{q}$, $\tau_{\mathbf{q}}$ decreases only by 9%, *i.e.* the contribution of the $1/\sqrt{\tau_{\mathbf{q}}}$ factor to $Z_1(\mathbf{q})$ is roughly constant. On the other hand, $g_{\mathbf{q}}$ strongly increases as q increases. Indeed, we computed for 5CB at $h = 0$ that $Z_1(q_c\hat{\mathbf{x}}) = 1.82, Z_1(q_{\rm f}\ \hat{\mathbf{x}}) = 1.69, Z_1(q_{\rm f}\ \hat{\mathbf{x}} + p_{\rm f}\ \hat{\mathbf{y}}) = 1.64$: first an increase of q by only 6% leads to a decrease by 7.3% of Z_1, and second going from 0 to finite p decreases only slightly, by 2.8%, the value of Z_1. From a diagram as in Figure 1 we found that the main effect of the increase of q is a strong increase of the contributions (P1) and (P4) to $g_{\mathbf{q}}$. This is understandable because these contributions are driven by gradients along x, *i.e.* they contain an explicit factor q.

The study of the saturation coefficient can also be performed in the subcritical regime $4.5 < h < 25$ where $g_{\mathbf{q}}$ becomes negative, a regime predicted in [8] and tentatively explained by some anti-saturating nonlinear magnetic terms in the n_z equation. We have found that these terms do contribute to change the sign of $g_{\mathbf{q}}$, but only as a secondary effect, since the contribution (N1) above is of much larger absolute value at intermediate h [18]. The subcritical bifurcation thus appears to be more linked to the fact that the cubic nonlinearities implying the velocity field, which are globally anti-saturating, become more important at intermediate h.

5 Slow dynamics of the roll modulations

The dynamics of a wave-packet

$$V = \int_{\mathcal{V}(\mathbf{q}_c)} d\mathbf{q}A(\mathbf{q})V_1(\mathbf{q}) + c.c. + h.o.t. \simeq A(\mathbf{r})V_1(\mathbf{q}_c) + c.c. + h.o.t. \tag{5.1}$$

with the slowly varying envelope

$$A(\mathbf{r}) = \int_{\mathcal{V}(\mathbf{q}_c)} d\mathbf{q}A(\mathbf{q})\exp(i(\mathbf{q}-\mathbf{q}_c)\cdot\mathbf{r}) \tag{5.2}$$

can be described by the following extension of the amplitude equation (4.10) (see [2,8,11,12]):

$$\tau\partial_t A(\mathbf{r}) = \epsilon A(\mathbf{r}) - \epsilon_0(\mathbf{q}_c + \hat{\mathbf{x}}i\partial_x + \hat{\mathbf{y}}i\partial_y)A(\mathbf{r}) - |A(\mathbf{r})|^2 A(\mathbf{r}). \tag{5.3}$$

We will now show that this lowest order envelope equation allows a first evaluation of the *relaxation times of the roll modulations*, which nearly diverge in the DDR.

For simplicity, we focus on the possible modulations of the critical rolls, given by the solution $A(\mathbf{r}) = \sqrt{\epsilon}$

of (5.3). Because of the cubic term $|A(\mathbf{r})|^2 A(\mathbf{r})$ in (5.3), a general long-wavelength perturbation is characterized by a modulation wavevector $\mathbf{s}$ and two small amplitudes $a_\pm$ (hereafter assumed real):

$$A(\mathbf{r}) = \sqrt{\epsilon} + a_+ \exp(i\mathbf{s}\cdot\mathbf{r}) + a_- \exp(-i\mathbf{s}\cdot\mathbf{r}). \qquad (5.4)$$

To lowest order, (5.3) gives

$$\tau\partial_t a_+ = -(\epsilon_0(\mathbf{q}_c+\mathbf{s})+\epsilon)\ a_+ - \epsilon a_-$$
$$\tau\partial_t a_- = -(\epsilon_0(\mathbf{q}_c-\mathbf{s})+\epsilon)\ a_- - \epsilon a_+.$$

Since $\epsilon_0(\mathbf{q}_c+\mathbf{s})$ and $\epsilon_0(\mathbf{q}_c-\mathbf{s})$ are close to each other, the most dangerous perturbation corresponds to $a_+ \simeq -a_-$, and yields a growth rate

$$\tau\sigma_{lw} = -\frac{\epsilon_0(\mathbf{q}_c+\mathbf{s})+\epsilon_0(\mathbf{q}_c-\mathbf{s})}{2} + \sqrt{\epsilon^2 + \Big(\frac{\epsilon_0(\mathbf{q}_c+\mathbf{s})-\epsilon_0(\mathbf{q}_c-\mathbf{s})}{2}\Big)^2} - \epsilon.$$

In the case of critical NR and to lowest order, the reduced thresholds $\epsilon_0(\mathbf{q}_c \pm \mathbf{s})$ are equal, and consequently

$$\tau\sigma_{lw} = -\epsilon_0(\mathbf{q}_c \pm \mathbf{s}). \qquad (5.5)$$

In the general case, assuming for instance $\epsilon_0(\mathbf{q}_c+\mathbf{s}) \leq \epsilon_0(\mathbf{q}_c-\mathbf{s})$, one gets immediately for the corresponding relaxation time $\tau_{lw} = -1/\sigma_{lw}$:

$$\frac{\tau}{\epsilon_0(\mathbf{q}_c-\mathbf{s})} \leq \tau_{lw} \leq \frac{\tau}{\epsilon_0(\mathbf{q}_c+\mathbf{s})}.$$

Because $\epsilon_0(\mathbf{q}_c+\mathbf{s})$ is minimal at $\mathbf{s}=\mathbf{0}$, and in finite-size experiments the smallest possible wavevector is the inverse δq of the aspect ratio (see Eq. (2.2) of [10]), one obtains for the maximum relaxation time of roll modulations:

$$\max \tau_{lw} \simeq \frac{\tau}{\min\limits_{|\mathbf{s}|=\delta q} \epsilon_0(\mathbf{q}_c+\mathbf{s})}\cdot \qquad (5.6)$$

This yields typically very long times at $h=0$ for the zig-zag modulations, *e.g.* for 5CB with equation 3.22, $\xi_{yy} = 0.46$ and $\delta q = 0.038$ for our experimental cell 3:

$$\tau_{lw} \simeq \frac{18 \text{ minutes}}{3\ 10^{-4}} \simeq 40 \text{ days!}$$

We will show in Section 3 of [10] that experimental measurements of the decay rate of undulated rolls at finite h agree well with the estimation (5.5); this agreement shows that the higher order corrections to (5.3) can really be neglected at very small ϵ. At $h=0$, the extremely large value of τ_{lw} then explains why the undulated rolls observed experimentally at threshold appear as "metastable" (see Sect. 3 of [10]).

We also expect from our results of Section 3.2 and from (5.6) that for a liquid crystal such that N4 a clear selection of OR might not be observable even at $h=0$, since the modulations in the y direction will still show a very slow dynamics.

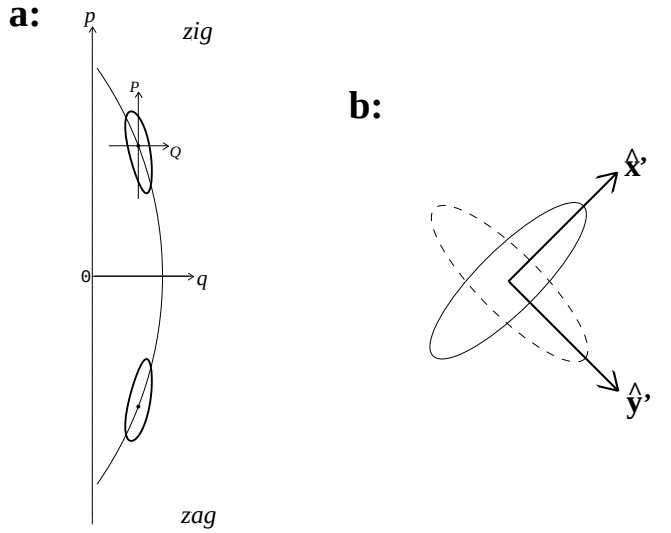

Fig. 2. (a) Geometry of the reduced threshold surface $\epsilon_0(\mathbf{q})$ for nematic convection in the oblique roll case, when $\epsilon_0(\mathbf{q})$ cancels in two symmetric points $\mathbf{q}_c$ (upper point) and $S(\mathbf{q}_c)$ (lower point). A non connex level line of $\epsilon_0(\mathbf{q})$ is shown (thick line). The low values of $\epsilon_0(\mathbf{q})$ are obtained only for wavevectors of modulus close to 1 (thin line: circle $|\mathbf{q}|=1$). Consequently when $Q = q - q_c$ and $P = p - p_c$ together increase, $\epsilon_0(\mathbf{q})$ is increased, as indicated by the positive correction $2a\xi_{xx}\xi_{yy}QP$ in (6.2). (b) Sketch of the level lines of $|A|$ (continuous line) and B (dashed line) in point-defect solutions of (6.3) in the case of anisotropic diffusion ($a>0$).

6 Localized competition between zig and zag roll modes

The nucleation of zig rolls in point defects of zag rolls described in Section 4.1 of [10], and shown on Figure 8a of [10], had not been modeled up to now. This effect has some similarities with localized effects studied by Coullet *et al.* in nonlinear waves [19], in Rayleigh-Bénard convection [20] or in mixing layers [21]. The competition between two symmetric variants (like the zig and the zag) has only been studied to our knowledge in [19]. There the situation is different from ours since the primary bifurcation is of the Hopf type, and this induces advection terms in the amplitude equations (of the type $c\partial_x A$). Consequently, in the exclusion regime (when the two variants exclude each other, *i.e.* when $g_2 > 1$, see below), no nucleation effects were predicted. We will show that things differ in our case of a primary stationary bifurcation.

Assuming that the zig-zags are obtained readily at threshold, we use the lowest-order envelope equations model [22], which governs the dynamics of the superposition

$$V \simeq [A(\mathbf{r})V_1(\mathbf{q}_c) + c.c.] + [B(\mathbf{r})V_1(S(\mathbf{q}_c)) + c.c.] + h.o.t. \qquad (6.1)$$

where A and B are respectively the envelope of the zig and the zag. Like in (5.3), an expansion of $\epsilon_0(\mathbf{q}_c + Q\hat{\mathbf{x}} + P\hat{\mathbf{y}})$

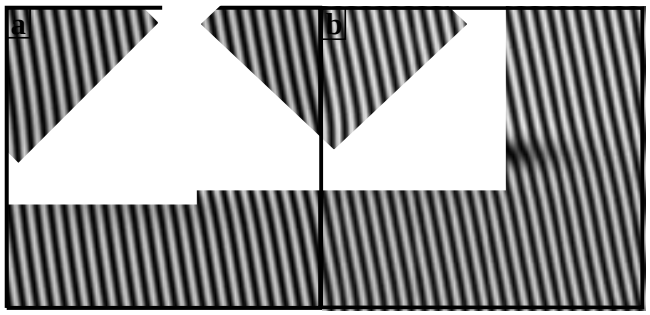

Fig. 3. (a) Zig point-defect observed in a simulation of coupled amplitude equations of the type (6.3), but where we have reintroduced the coherence lengths ξ_{xx} and ξ_{yy} in order to reproduce the experimental situation. The values of the parameters are $\xi_{xx} = 0.48$, $\xi_{yy} = 0.17$, $a = 0.30$, $g_2 = 1.34$, $\epsilon = 0.05$. In the core of the zig point-defect (center of the image where $A = 0$), $|B|$ is maximum, and one observes some zag-like rolls. The "effective" core of the dislocation, where the local fields cancel, appears to the right of the point $A = 0$. (b) Point defect observed in a simulation of a unique amplitude equation of the type (5.3) where the growth rate presents two symmetric maxima associated with the zig and the zag (see text). The defect of zig is strongly dissymetric, and the nucleation of the zag has developed spontaneously, with the same phase coherence as in the experiments.

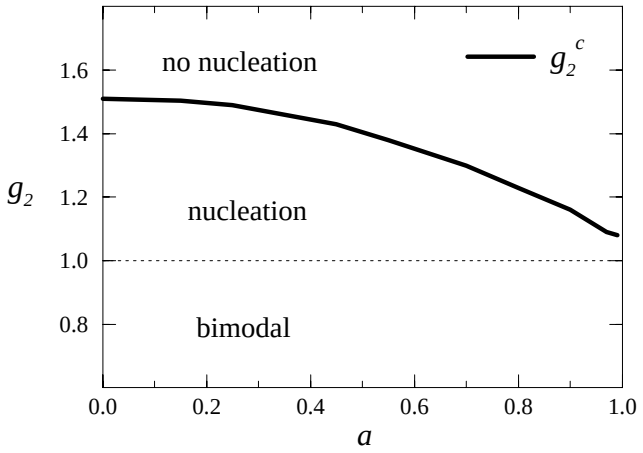

Fig. 4. As a function of the coefficient of anisotropy a, critical value of the nonlinear coupling coefficient g_2 between the zig and the zag rolls (see Eq. (6.3)) under which a nucleation develops in point defects.

is required, now

$$\epsilon_0(\mathbf{q}_c + Q\hat{\mathbf{x}} + P\hat{\mathbf{y}}) \simeq \xi_{xx}^2 Q^2 + \xi_{yy}^2 P^2 + 2a\xi_{xx}\xi_{yy} QP \tag{6.2}$$

with a a coefficient of anisotropy. This coefficient is positive for OR in nematic convection, since the modulus of the wavevector should always stay close to 1 (see Fig. 2a for an explanation of the sign of a). Rescaling the horizontal coordinates x and y by ξ_{xx} and ξ_{yy}, one obtains [22]:

$$\begin{aligned}
\tau\partial_t A(\mathbf{r}) &= (\epsilon + \partial_x^2 + \partial_y^2 + 2a\partial_x\partial_y)\ A(\mathbf{r}) \\
&\quad - |A(\mathbf{r})|^2 A(\mathbf{r}) - g_2|B(\mathbf{r})|^2 A(\mathbf{r}) \\
\tau\partial_t B(\mathbf{r}) &= (\epsilon + \partial_x^2 + \partial_y^2 - 2a\partial_x\partial_y)\ B(\mathbf{r}) \\
&\quad - |B(\mathbf{r})|^2 B(\mathbf{r}) - g_2|A(\mathbf{r})|^2 B(\mathbf{r}).
\end{aligned} \tag{6.3}$$

We have performed numerical simulations of (6.3) in the exclusion regime $g_2 > 1$, where the spatially homogeneous, stationary stable solutions are either $A = \sqrt{\epsilon}, B = 0$ (pure zig) or $A = 0, B = \sqrt{\epsilon}$ (pure zag). When the exclusion is not too strong, *i.e. when the nonlinear competition coefficient g_2 is below some critical value $g_2^c(a)$* (but still > 1), *some nucleation effects develop.*

We use a finite-difference code, on grids of various sizes (from 64×64 to 256×256) in order to test the robustness of the results. All simulations are started with an approximate solution for a point defect of A:

$$A(\mathbf{r}) = \sqrt{\epsilon}\ \tanh\left(\sqrt{\frac{\epsilon}{2}}|\mathbf{r}|\right) \exp(i \arg \mathbf{r}) \tag{6.4}$$

where the center of the coordinates is the center of the grid, and with some noise for B. The boundary conditions are $\nabla A = 0$, in order to prevent the defect from moving to the sides, and $B = 0$. A stationary solution is always obtained after a certain time. For $g_2 > g_2^c(a)$, in the final point-defect solution B has everywhere relaxed to zero, whereas A has only slightly varied from the simple ansatz (6.4). On the contrary, for $g_2 < g_2^c(a)$, a small bump of B has developed, centered at the core of the defect, where $A = 0$. Inside this bump, the phase of B is homogeneous, but arbitrary. Note also that in the core of the defect $|A|$ has decreased as compared with a solution at higher g_2, of course due to the presence of B. The profiles of $|A|$ and $|B|$ look like in the Figure 4 of [19], but now the asymptotic value of $|B|$ far from the defect is zero and not a constant. If we reconstruct the field $n_z^2(\mathbf{r})$ from (6.1), with an adequate choice of phase (B real negative), we obtain as a typical result the image of Figure 3a, which shows great similarities with the experimental defects (compare with Fig. 8a of [10]).

If g_2 approaches 1 from above, the area where $|B|$ is nonzero and $|A|$ is decreased increases. In fact, when $g_2 = 1$, the asymptotic values of the amplitude must reach the bimodal values $|A| = |B| = \sqrt{\epsilon}/2$.

The dependence of g_2^c on a (Fig. 4) can be understood as follows: a characterizes the anisotropic diffusion of $A(\mathbf{r})$ and $B(\mathbf{r})$, which is preferential in symmetric directions for A and B. Indeed, if we introduce a new orthonormal coordinate system (x', y') such that $\hat{\mathbf{x}}'$ points in the direction of the bisector of $\hat{\mathbf{x}}$ and $\hat{\mathbf{y}}$, the diffusion terms in (6.3) become:

$$\begin{aligned}
\tau\partial_t A(\mathbf{r}) &= [\epsilon + (1+a)\partial_{x'}^2 + (1-a)\partial_{y'}^2]\ A(\mathbf{r}), \\
\tau\partial_t B(\mathbf{r}) &= [\epsilon + (1-a)\partial_{x'}^2 + (1+a)\partial_{y'}^2]\ B(\mathbf{r}).
\end{aligned}$$

Since $a > 0$, A diffuses preferentially in the direction $\hat{\mathbf{x}}'$, whereas B diffuses preferentially in the direction $S(\hat{\mathbf{x}}')$. Typically, the level lines of $|A|$ will therefore be ellipses

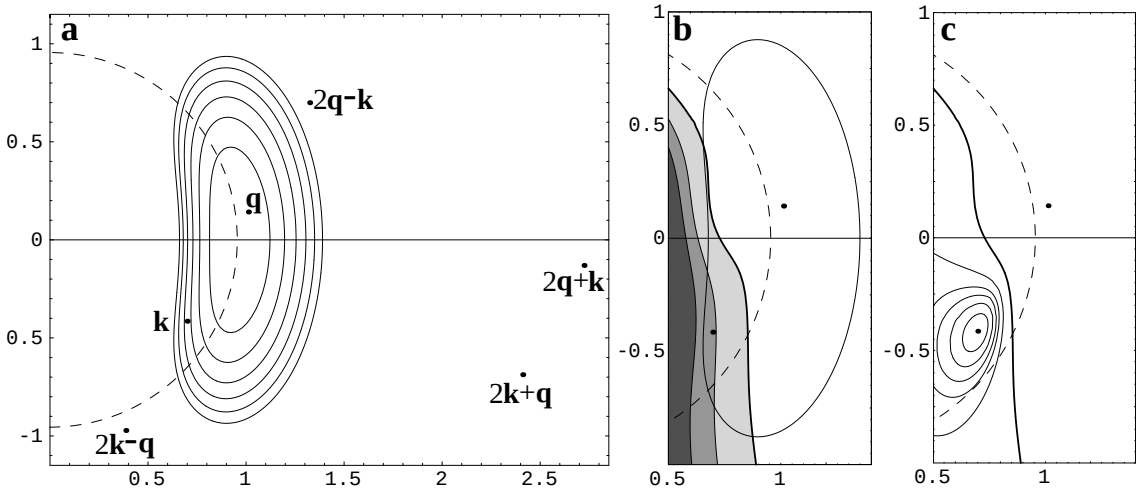

Fig. 5. (a) Geometry in Fourier space of the bimodal varicose calculated for 5CB at $h = 0$ and for a representative oblique-roll wavevector $\mathbf{q} = \mathbf{q}_f = 1.07 q_c(\hat{\mathbf{x}} \cos 8^\circ + \hat{\mathbf{y}} \sin 8^\circ)$ (Eq. (4.3) of [10]). The dual wavevector $\mathbf{k}$ is shown, together with the wavevectors of the cubic combinations of the basic modes in (7.1) which have the $z-$symmetry of the linear active modes. These modes are inactive because their wavevectors lie outside the active region, determined by the level lines $0.06, 0.12, ..., 0.36$ of $\epsilon_0(\mathbf{k})$. Note that the active region is roughly centered around the circle $|\mathbf{k}| = q_c$ (dashed line). (b) In the active area (the level line 0.36 of $\epsilon_0(\mathbf{k})$ has been reproduced), level lines 1 (thick line), $0, -1$ (thin lines) of the bimodal coupling coefficient $g_{\mathbf{qk}}$. **c**: resulting level lines $0.194, 0.205, 0.22, 0.24, 0.30$ (thin lines) and $+\infty$ (thick line) of $\epsilon_V(\mathbf{q}; \mathbf{k})$ in the same area.

of long axis along $\hat{\mathbf{x}}'$, whereas the level lines of $|B|$ will be ellipses of long axis along $S(\hat{\mathbf{x}}')$. The eccentricity of these ellipses increasing with a, larger a values imply that B will encounter in the direction $S(\hat{\mathbf{x}}')$ larger $|A|$ values, *i.e.* that the effective damping of B by A will be stronger (see Fig. 2b for a sketch of this mechanism). To nevertheless allow for a nucleation of B in the core of a defect of A, $g_2^c(a)$ should therefore be smaller at higher a (Fig. 4).

Note that a systematic calculation of the coefficients in (6.3) from the basic equations (with a method analogous to the one exposed in Sect. 4) gives typically, at low h, $1.5 \lesssim g_2 \lesssim 2.0$: one finds too large g_2 values for the nucleation. This result, together with the fact that only properly chosen phase shifts between A and B are needed to reconstruct the experimental defects, indicates that the real situation is more complex than the one described by the model (6.3). Nevertheless, as shown in Figure 3b, the nucleation effects also develop in simulations of a single envelope equation containing the two zig-zag modes (an equation like (5.3), but where $\epsilon_0(\mathbf{q})$ presents two minima at $q_c\hat{\mathbf{x}} \pm p_c\hat{\mathbf{y}}$). Therefore these nucleation effects appear to be rather generic.

7 Secondary bifurcation from oblique rolls to bimodal varicose

Bimodal secondary instabilities in planar nematic convection have been observed for a long time in electroconvection [23] and were also reported to occur in thermoconvection at very low [9,10] or intermediate h [6]. For their modeling, we derive as in Section 4.1 the corresponding amplitude equations, using as a basic ansatz

$$V = A\ V_1(\mathbf{q}) + \overline{A}\ V_1(-\mathbf{q}) + B\ V_1(\mathbf{k}) + \overline{B}\ V_1(-\mathbf{k}) + V_2. \tag{7.1}$$

There $\mathbf{q}$ is a typical zig wavevector; the case of a zag follows immediately by application of S: $\hat{\mathbf{y}} \mapsto -\hat{\mathbf{y}}$. The mode $\mathbf{q}$ is assumed to be stable against long-wavelength perturbations, as observed in the experiments, and confirmed by recent fully nonlinear calculations [24]. $\mathbf{k}$ is a secondary wavevector which might be the dual of $\mathbf{q}$ (see the definitions in [9] and Eq. (7.5) below). The second harmonics read now

$$\begin{aligned} V_2 = {} & |A|^2\ V_2(\mathbf{q}, -\mathbf{q}) + [A^2\ V_2(\mathbf{q}, \mathbf{q}) + c.c.] \\ & + [AB\ V_2(\mathbf{q}, \mathbf{k}) + \overline{A}B\ V_2(-\mathbf{q}, \mathbf{k}) + c.c.] + O(B^2) \end{aligned} \tag{7.2}$$

with definitions analogous to (4.3, 4.4). As shown in Figure 5a, the wavevectors $\mathbf{q}$ and $\mathbf{k}$ are typically far apart. Consequently, the mode at $2\mathbf{q} - \mathbf{k}$, obtained by combinations of active modes in cubic order, and therefore of the $z-$symmetry of the active modes (*cf.* Eq. (2.22)), is inactive. Here is an important difference with the case of a long-wavelength varicose instability at onset, where $\mathbf{s} = \mathbf{k} - \mathbf{q}$ is small, and therefore the structure is a "trimodal" $\{\mathbf{q}, \mathbf{q}+\mathbf{s}, \mathbf{q}-\mathbf{s}\}$ or $\{\mathbf{q}, \mathbf{k}, 2\mathbf{q}-\mathbf{k}\}$ of the type (5.4). In our "bimodal" case, the active amplitude equations are only obtained by projection of (2.20) on $U_1(\mathbf{q})$ and $U_1(\mathbf{k})$ respectively:

$$\begin{aligned} \tau_{\mathbf{q}} \partial_t A &= \epsilon\ A - |A|^2 A - g_{\mathbf{kq}} |B|^2 A, \\ \tau_{\mathbf{k}} \partial_t B &= (\epsilon - \epsilon_0(\mathbf{k}))B - |B|^2 B - g_{\mathbf{qk}} |A|^2 B. \end{aligned} \tag{7.3}$$

We have neglected in the equation for A the contribution of the linear threshold $\epsilon_0(\mathbf{q})$, since the primary mode in

the bimodal is always rather close to $\mathbf{q}_c$. The relevant nonlinear coefficient is $g_{\mathbf{qk}}$, which measures the feedback exerted by the modes contained in (7.1) on the mode $\mathbf{k}$:

$$g_{\mathbf{qk}} = \; - \; \tau_{\mathbf{k}} \; \langle U_1(\mathbf{k}), T_{\mathbf{qk}} \rangle$$

where

$$\begin{aligned} T_{\mathbf{qk}} = & \, N_2(V_1(-\mathbf{q})|V_2(\mathbf{q},\mathbf{k})) \\ & + N_2(V_1(\mathbf{q})|V_2(-\mathbf{q},\mathbf{k})) \\ & + N_2(V_2(\mathbf{q},-\mathbf{q})|V_1(\mathbf{k})) \\ & + N_3(V_1(\mathbf{q})|V_1(-\mathbf{q})|V_1(\mathbf{k})). \end{aligned} \tag{7.4}$$

The OR $\mathbf{q}$ solution of (7.3), $A = \sqrt{\epsilon}, B = 0$, loses stability against fluctuations of B, *i.e.* against a bimodal varicose $(\mathbf{q};\mathbf{k})$, only if $g_{\mathbf{qk}} < 1$, and for ϵ then larger than

$$\epsilon_V(\mathbf{q};\mathbf{k}) = \frac{\epsilon_0(\mathbf{k})}{1 - g_{\mathbf{qk}}} \cdot \tag{7.5}$$

The active mode $\mathbf{k}$ which minimizes this secondary threshold is the dual of $\mathbf{q}$. In the case of a primary supercritical instability, the comparison of (7.4) with (4.8) shows that $g_{\mathbf{qk}} \to 2$ when $\mathbf{k} \to \mathbf{q}$, *i.e.* that nearby wavevectors always exclude each others. On the other hand, for all nematic parameters, when $\mathbf{k}$ moves away from $\mathbf{q}$ in the zag region, $g_{\mathbf{qk}}$ reaches strongly negative values which favor the bimodal instability (see Fig. 5b for the example of 5CB). The position of the dual mode is then selected by a balance between the nonlinear interaction factor $(1 - g_{\mathbf{qk}})^{-1}$, which favors $\mathbf{k}$ far from $\mathbf{q}$, and the linear "cost" $\epsilon_0(\mathbf{k})$ of the mode $\mathbf{k}$, which favors $\mathbf{k}$ close to $\mathbf{q}$ (in particular, preferentially $|\mathbf{k}| \simeq |\mathbf{q}|$). The calculations must be performed at a value of ϵ close to the value of the resulting bimodal threshold to be valid [25]; we used to fix ϵ at $\epsilon_0(\mathbf{q})$. For 5CB at $h = 0$ and the primary zig mode $\mathbf{q} = \mathbf{q}_f$ (Sect. 4.3 of [10]), experimental measurements (see Eq. (4.8) and Fig. 9b of [10]) have shown that the corresponding dual mode is given by $|\mathbf{k}| \simeq 0.9|\mathbf{q}|, \arg \mathbf{k} \simeq -55°$, and that the threshold for homogeneous bimodal varicose is $\epsilon_V \simeq 0.28$. From our calculations a semi-quantitative agreement is obtained with $|\mathbf{k}| = 0.80|\mathbf{q}|, \arg \mathbf{k} = -31°, \epsilon_V = 0.19$. Still at $h = 0$ we find for MBBA at $|\mathbf{q}| = 1.07 q_c, \arg \mathbf{q} = 10°$ (*cf.* Eq. (4.3) of [10]), $|\mathbf{k}| = 0.79|\mathbf{q}|, \arg \mathbf{k} = -33°, \epsilon_V = 0.25$, which agree qualitatively with the experimental measurements (Eq. (4.8) of [10]), and $\epsilon_V \simeq 0.38$. Finally for N4 at $\mathbf{q} = \mathbf{q}_c$ we predict $|\mathbf{k}| = 0.99|\mathbf{q}|, \arg \mathbf{k} = -41°, \epsilon_V = 0.12$.

In order to find the origin of the bimodal varicose instability, the diagram for $g_{\mathbf{qk}}$ (7.4) can be constructed (Fig. 2 of [26]), which is complex since many contributions appear to control the value of $g_{\mathbf{qk}}$. In particular, the same cubic nonlinearities as those implied in the saturation, $-F(\partial_x v_z + \partial_z v_x) n_z^2$ (*cf.* the contributions (P3) and (N1) of Sect. 4.2), now coupling $V_1(\mathbf{q}), V_1(-\mathbf{q})$ and $V_1(\mathbf{k})$, are important. This can be explained by the fact that replacing one $V_1(\mathbf{q})$ by $V_1(\mathbf{k})$ in (P3) or (N1) leads to a contribution in $g_{\mathbf{qk}}$ analog to the corresponding contribution in $g_{\mathbf{q}}$, since $\mathbf{k}$ is not so far from $\mathbf{q}$. Thus, self-saturating or anti-saturating effects typically also contribute to damp or excite other wavevectors in the bimodal

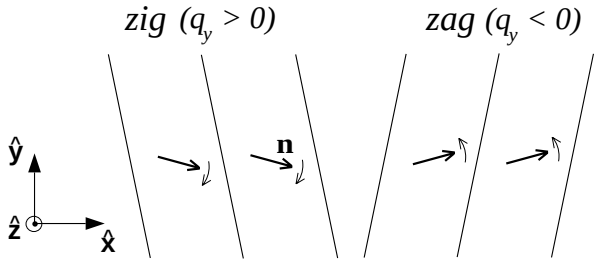

Fig. 6. Sketch of the rotation of the director in oblique rolls expressed by the component $\tilde{n}_y^H S_1(z)$ of the horizontally homogeneous second harmonics $V_2(\mathbf{q},-\mathbf{q})$. $\tilde{n}_y^H$ is negative for a zig and positive for a zag: the director rotates in the direction of the axis of the rolls.

secondary instability. Some quadratic nonlinearities give also important contributions to $g_{\mathbf{qk}}$, *e.g.* advection terms in $N_{2n_z}(V_1(\mathbf{q})|V_2(-\mathbf{q},\mathbf{k}))$. They are difficult to interpret since the second harmonics $V_2(-\mathbf{q},\mathbf{k})$ has a complicated structure. However, a reduction of the complexity can be achieved by forming the difference $\delta g_{\mathbf{qk}} = g_{\mathbf{qk}} - g_{\mathbf{q}S(\mathbf{k})}$, which is negative and thus expresses that zag duals are preferred to zig duals. This shows [26] that two terms only select the symmetry (zig or zag) of the dual mode: the term in $N_{2\theta}(V_2(\mathbf{q},-\mathbf{q}), V_1(\mathbf{k}))$:

$$-R\kappa_a \partial_y (n_y n_z) = +R\kappa_a \tilde{n}_y^H(\mathbf{q}) \; k_y \tilde{n}_z(\mathbf{k}) \; S_1^2(z) \exp(i\mathbf{k}\cdot\mathbf{r}) \tag{7.6}$$

and the α_2 term in $N_{2n_z}(V_2(\mathbf{q},-\mathbf{q}), V_1(\mathbf{k}))$:

$$F n_y \, \partial_y v_z = F \tilde{n}_y^H(\mathbf{q}) \, i \, k_y \mathbf{k}^2 \, \tilde{f}(\mathbf{k}) \; S_1(z) C_1(z) \exp(i\mathbf{k}\cdot\mathbf{r}) \tag{7.7}$$

where we have used (4.3, 3.2).

In order to understand the corresponding mechanisms, we first study the quadratic effect expressed by $\tilde{n}_y^H$. The nonzero amplitude of the n_y field in $V_2(\mathbf{q},-\mathbf{q})$ expresses a rotation of the director in the horizontal plane, homogeneous in x, y, and with a z-profile in $S_1(z) = \cos z$ such that the rotation is maximal at the mid-plane of the layer. This rotation must occur in symmetric directions for the zig and the zag because of the rule (2.21) (*cf.* Fig. 6). Since the temperature and the director fields are not coupled for horizontally homogeneous distortions, (4.3) gives directly

$$\tilde{n}_y^H = \frac{F}{k_{22}} \sum_l \left\langle S_1 | N_{2n_y l}(V_1(\mathbf{q})|V_1(-\mathbf{q})) \right\rangle \tag{7.8}$$

where the nonlinear terms in the n_y equation are labeled with an index l. The corresponding diagram, calculated for 5CB and the typical zig wavevector (Eq. (4.3) of [10]) (Fig. 7), shows that 3 nonlinearities in the n_y equation impose the negative value of $\tilde{n}_y^H$ in zigs:

(H1) the advection term $-F v_z \partial_z n_y$;
(H2) the α_2 term $-F(\partial_x v_x^f) n_y$, where only the f part of v_x (Eq. (B.1)) must be considered;
(H3) the α_2 term $F(\partial_z v_y^f) n_z$, where only the f part of v_y (Eq. (B.1)) must be considered.

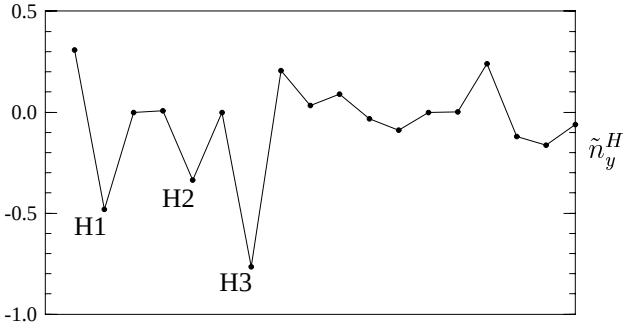

Fig. 7. Diagram of the 18 contributions (7.8) to $\tilde{n}_y^H = -1.17$ in the zig mode at $\mathbf{q} = \mathbf{q}_f$ (Eq. (4.3) of [10]) in 5CB. The most important contributions are indicated with the labels H1 to H3.

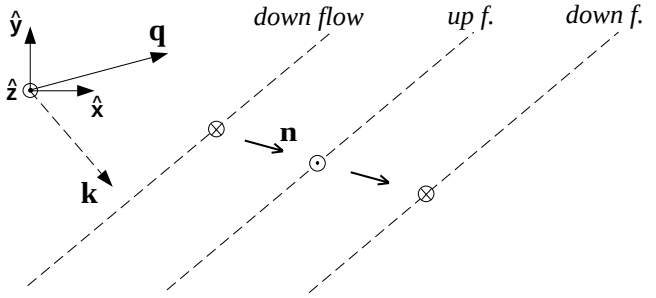

Fig. 8. Sketch of one of the mechanisms selecting the dual wavevector in the bimodal varicose, expressed by the coupling term (7.7) between the homogeneous n_y component due to the presence of a zig $\mathbf{q}$ mode ($\leftrightarrow$ rotated director) and a vertical velocity $\mathbf{k}$ mode, with $\mathbf{k}$ zag ($\leftrightarrow$ up and down flows). In the left roll, $n_y(\mathbf{q})$ and $\partial_y v_z(\mathbf{k})$ negative induce a positive n_z component; in the right roll, $n_y(\mathbf{q})$ and $\partial_y v_z(\mathbf{k})$ opposed to each other induce a negative n_z component. This $n_z(\mathbf{k})$ mode is in phase with the one induced by the linear instability mechanism for the $\mathbf{k}$ mode (by the $\partial_x v_z$ term in the n_z equation).

The fact that advection plays a role is not surprising, since it tends to homogenize spatially the fields. However, the sign of $\tilde{n}_y^H(\mathbf{q})$ seems to be controlled mostly by the α_2 terms (H2) and (H3) (Fig. 7), in agreement with the general interpretation of the α_2 effects on the director dynamics given in Section 2.1. Indeed, the simplest way to minimize the director-transverse velocity gradients in a roll structure is to rotate the director towards the axis of the rolls: in this direction there are no more velocity gradients because of the translational invariance. More quantitatively, one can approximate at small $p = \mathbf{q}\cdot\hat{\mathbf{y}}$, $|p| \lesssim 0.16$, $\tilde{n}_y^H(\mathbf{q})$ by a linear expansion in p, because of the symmetry rule $\tilde{n}_y^H(\mathbf{q}) = -\tilde{n}_y^H(S(\mathbf{q}))$. Thus the homogeneous part of the director field in the WNL oblique roll solutions (4.1) can be approximated at small p by

$$n_y = Y_1(q)\ p\ (\epsilon - \epsilon_0(\mathbf{q}))\ S_1(z) \tag{7.9}$$

where $q = \mathbf{q}\cdot\hat{\mathbf{x}}$, and at $h = 0$:

$$\begin{aligned} &Y_1(q_c) = -8.2\ \ ,\ Y_1(1.06q_c) = -7.1 \quad \text{for MBBA,}\\ &Y_1(q_c) = -10.2\ ,\ Y_1(1.06q_c) = -8.3 \quad \text{for 5CB,}\\ &Y_1(q_c) = -13.6\ ,\ Y_1(1.06q_c) = -12.8 \quad \text{for N4.} \end{aligned} \tag{7.10}$$

Note that for $q_c < q < 1.06q_c$, a linear expansion of $Y_1(q)$ is valid. The amplitude Y_1 decreases with increasing q mainly because of the decrease of the convective amplitude Z_1 studied in Section 4.2. Indeed, one expects from (7.8, 4.9, 4.14) that $\tilde{n}_y^H, Y_1 \propto (Z_1)^2$. Note finally that N4 is the nematic where a stronger rotation occurs, because of its high anisotropy (Appendix A).

We can now understand the mechanism expressed by (7.7) for instance as sketched in Figure 8: the rotation of the director in the $-\hat{\mathbf{y}}$ direction inside OR zig makes the director sensitive to the vertical shear along $\hat{\mathbf{y}}$, and thus a fluctuation of vertical velocity of wavevector $\mathbf{k}$ nonlinearly enhances the corresponding n_z mode of wavevector $\mathbf{k}$. In fact, term (7.7) is a correction to the shear term $\partial_x v_z$ in the n_z equation, which is one of the terms responsible of the anisotropic convection mechanism. Equivalently, (7.6) expresses that a n_z fluctuation of wavevector $\mathbf{k}$ nonlinearly enhances the corresponding temperature mode of wavevector $\mathbf{k}$. This term (7.6) is also a correction to a linear term responsible of the convection mechanism, namely the heat-focusing term $-R\kappa_a\partial_x n_z$ in the heat equation. Therefore these two mechanisms can be explained as follows: if the average director orientation has changed, and if one still injects some energy in the system by increasing ϵ, a new mode roughly parallel to the new direction of the director will be excited by the focusing mechanism.

We conclude by reviewing other features of the model (7.3). If one assumes a bifurcation to zig-zags at threshold, and if $g_{\mathbf{q}_c S(\mathbf{q}_c)} < 1$, then the dual of $\mathbf{q}_c$ *must* be $S(\mathbf{q}_c)$, since $\epsilon_0(S(\mathbf{q}_c)) = 0$ implies according to (7.5) that $\epsilon_V(\mathbf{q}_c; S(\mathbf{q}_c)) = 0$ is minimal. From the principle that close wavevectors exclude each other, one expects that $g_{\mathbf{q}_c S(\mathbf{q}_c)}$ can become smaller than 1 only when the zig and zag modes are far apart, *i.e.* when the angle $\arg\mathbf{q}_c$ is close to 45°. Indeed, one finds for 5CB, in the upper supercritical region $h > 25$, where $\arg\mathbf{q}_c(h)$ increases from 11° to 90°, that $g_{\mathbf{q}_c S(\mathbf{q}_c)} < 1$ from $h = 25$ (where the vicinity of the subcritical region narrows the WNL domain) but only up to $h = 30$. At higher h, $\arg\mathbf{q}_c(h)$ is larger than 60°, $\mathbf{q}_c$ and $-S(\mathbf{q}_c)$ become close and exclude each other. Indeed, experiments in thermoconvection at high h have shown a bimodal at threshold only for $25 \lesssim h \lesssim 30$ [6]. Finally, the simple structure of (7.3) allows to calculate analytically the amplitudes in the bimodal varicose:

$$\begin{aligned} |A| &= \sqrt{\epsilon - r\, g_{\mathbf{kq}}\,(\epsilon - \epsilon_V)}\\ |B| &= \sqrt{r\,(\epsilon - \epsilon_V)} \end{aligned} \tag{7.11}$$

where $r = (1-g_{\mathbf{qk}})/(1-g_{\mathbf{qk}}g_{\mathbf{kq}})$ is positive in the interesting cases. These solutions are stable against perturbations in δA and δB of (7.3). Thus we confirm some measurements of the pinching amplitude in the bimodal varicose, which gave access directly to $|B/A|$, and showed a law of the type $|B/A| \sim \sqrt{\epsilon - \epsilon_V}$ near the transition (see [23], and also the beginning of Sect. 4.3 of [10]).

8 Conclusion

A common feature of almost all the mechanisms put into evidence here (mechanisms (E2-E5) of Sect. 3.2, (P2-P4, N1) of Sect. 4.2, (7.7) and (H1-H3) of Sect. 7) is that they do not imply any coupling terms with the scalar field driving the convection (here the temperature field, in electroconvection it would be the charge density). Instead, these mechanisms always imply director effects, and more precisely in most of the cases hydrodynamical couplings between the director and the velocity fields. Therefore these mechanisms should develop identically in thermo- and electroconvection in the "director-dominated regimes" where the damping of the director field is very weak. We believe that this explains the high degree of similarity between these two systems. Also, our results prove the general importance of the α_2 viscous torque in planar convection in the nonlinear regime, and the relevance of our interpretation of Section 2 for this torque.

There are of course limitations to the results presented here, and certain extensions should be performed. First, the nucleation scenario in point defects has to be refined. In particular, we have not addressed the competition between the zig mode and modes close to its dual, which drives the interesting pre-transitional effects shown in Figure 8b of [10]. This is not a straightforward extension, since an expansion of the growth rate near the dual wavevector would lead in direct space to anti-diffusion terms. Second, we have found that, in WNL oblique rolls solutions, the contribution of $\tilde{n}_y^H$ in the second harmonics $V_2(\mathbf{q}, -\mathbf{q})$ (4.3) usually overcomes the contribution of $\tilde{n}_y$ in the roll mode $V_1(\mathbf{q})$ (3.2) at rather small ϵ values, $\epsilon < \epsilon_V$. Thus the second harmonics do not appear to be a small perturbation of the roll mode: the WNL scheme used here probably neglects important effects. An extension of this WNL scheme in order to include n_y effects up to cubic order should be performed. We note that such an extension has already been presented for the case of homeotropic electroconvection, where the homogeneous n_y mode appears obviously as a zero-mode [27]. In the planar case, such an extension would probably allow for the study of other n_y effects than those responsible for the bimodal varicose: we think of the recently discovered *abnormal rolls* [28], but also of the bimodal oscillations, which cannot be described by the model (7.3). Third, it would be interesting to include in this extended WNL scheme the study of the long-wavelength secondary instabilities of rolls, for which the results of the standard WNL scheme seem to be unreliable, according to our experiments and the work of [8,24].

Finally, the method of investigation of nonlinear mechanisms from the study of amplitude equation coefficients developed here might provide one starting point for understanding nonlinear phenomena. Indeed, this method could be applied to any other dynamical system where the basic "microscopic" equations are known.

We thank W. Pesch for useful discussions and for his careful reading of the manuscript. This work was supported by the Direction des Recherches et Etudes Techniques under contract DGA/DRET/94136. E.P. also acknowledges support from the DFG-Kr690/4-4 during his stay in Bayreuth where the manuscript was completed.

Appendix A: Material parameters

The nematics for which systematic measurements of the material parameters exist are to our knowledge:

1. MBBA = *N*-(*p*-methoxybenzylidene)-*p*-butylaniline, which presents a nematic phase between $T_S = 22$ °C and $T_{NI} = 46$ °C. Its anisotropic viscosities have been measured in [29,30], and its other material parameters in [31].
2. 5CB = 4-*n*-pentyl-4'-cyanobiphenyl, which presents a nematic phase between $T_S = 25$ °C and $T_{NI} = 35.2$ °C. Its material constants have been compiled by Ahlers in [2].
3. N4 = Merck Phase-4, which presents a nematic phase between $T_S = 16$ °C and $T_{NI} = 74.8$ °C. Its anisotropic viscosities have been measured in [29,30].
4. N5 = Merck Phase-5, which presents a nematic phase between $T_S = 5.15$ °C and $T_{NI} = 73.8$ °C. Its anisotropic viscosities have been measured in [32].

In order to support our approximation (2.7) for the coupling $\mathbf{v} \to \mathbf{n}$, Table 2 displays the average and extremal values of the ratio α_3/α_2. The dimensionless model parameters used in the calculations are in Table 3. We considered as standard nematic materials at room temperature MBBA and 5CB at 27 °C, used in [10]; and as a more anisotropic nematic N4 at 20 °C, with which new experiments are starting at Orsay. Indeed N4 shows a nematic phase covering a wide temperature range, and the anisotropy of a nematic typically increases when one decreases the temperature deep inside the nematic phase. For N4, we assumed reasonable values for the unknown parameters $Pr, F, \kappa'_a, k'_{22}, k'_{33}$ and α'_1, guided by the correspondence between these parameters and the anisotropic viscosities observed for MBBA and 5CB [33].

Table 2. Average and extremal values of the modulus of the ratio $\alpha_{32} = \alpha_3/\alpha_2$ based on the measurements of the viscosities of the liquid crystals (l.c.) MBBA, 5CB, N4, N5 as a function of the temperature. We have specified the value of the reduced temperature $T' := T - T_{NI}$, in degrees Celsius, at which the maximum value of α_{32} was measured.

l.c.	$\langle\lvert\alpha_{32}\rvert\rangle$	$\max\lvert\alpha_{32}\rvert$
MBBA	0.04	0.09 ($T' = -2$)
5CB	0.06	0.06 ($T' = -1.2$)
N4	0.05	0.14 ($T' = -0.8$)
N5	0.04	0.12 ($T' = -0.8$)

Table 3. Dimensionless parameters used for the nematic liquid crystals MBBA, 5CB and N4.

l.c.	Pr	F	κ_a'	k_{11}'	k_{22}'	k_{33}'	α_1'	α_2'	α_3'	α_4'	γ_3'	γ_4'	γ_5'
MBBA	395	1371	0.656	1	0.623	1.290	-0.438	-2.590	-0.036	2	0.412	2.215	0.376
5CB	440	790	0.663	1	0.634	1.303	-0.184	-2.343	-0.132	2	0.353	2.119	0.222
N4	450	900	0.99	1	0.503	1.495	0	-3.967	0.093	2	0.466	3.408	0.559

Appendix B: Velocity potentials

The velocity potentials used in the layer geometry were first introduced for the study of isotropic thermoconvection in [34]. For roll-modes of horizontal dependence in $\exp(i\mathbf{q}\cdot\mathbf{r})$, the assumed incompressibility of the fluid ($\nabla\cdot\mathbf{v}=0$) and the definition of the vertical vorticity $\Omega_z=\partial_x v_y-\partial_y v_x$ allow for expressing the horizontal velocity in terms of v_z and Ω_z:

$$v_x = iq\,\partial_z f + ip\,g\,,\quad v_y = ip\,\partial_z f - iq\,g, \tag{B.1}$$

with

$$f=\mathbf{q}^{-2}\,v_z\,,\quad g=\mathbf{q}^{-2}\,\Omega_z. \tag{B.2}$$

Another interpretation of these potentials is that, in such a roll structure, f controls the horizontal velocity perpendicular to the axis of the rolls:

$$v_\perp=\frac{\mathbf{q}}{|\mathbf{q}|}\cdot\mathbf{v}=i|\mathbf{q}|\,\partial_z f, \tag{B.3}$$

and g the horizontal velocity parallel to the axis of the rolls:

$$v_\parallel=\Big(\hat{\mathbf{z}}\times\frac{\mathbf{q}}{|\mathbf{q}|}\Big)\cdot\mathbf{v}=-i|\mathbf{q}|g. \tag{B.4}$$

Note that this "anomalous" velocity component cancels for the thermoconvection of isotropic fluids.

Appendix C: Galerkin technique - linear Galerkin equations

In the Galerkin technique the vertical dependence of the fields (see Sect. 2.2) is expanded in terms of test functions satisfying the boundary conditions at $z=\pm\pi/2$ due to our scaling conventions. The fields n_y, n_z, g and θ are expanded on the sine basis $S_n(z)=\sin(n(z+\pi/2))$, whereas f is expanded on the Chandrasekhar basis of functions. It is defined here as the solution of

$$\partial_z^4 C_n=\lambda_n^4 C_n \;\text{ and }\; C_n(z)=\partial_z C_n(z)=0 \text{ for } z=\pm\pi/2.$$

This gives, for the first Chandrasekhar functions,

$$C_1(z)=\frac{1}{\sqrt{2}}\Big(\frac{\cosh(\lambda_1 z)}{\cosh(\lambda_1\pi/2)}-\frac{\cos(\lambda_1 z)}{\cos(\lambda_1\pi/2)}\Big)$$
$$\text{with}\quad \lambda_1=1.50562,$$
$$C_2(z)=\frac{1}{\sqrt{2}}\Big(\frac{\sinh(\lambda_2 z)}{\sinh(\lambda_2\pi/2)}-\frac{\sin(\lambda_2 z)}{\sin(\lambda_2\pi/2)}\Big)$$
$$\text{with}\quad \lambda_2=2.49975.$$

The projected equations are obtained with the scalar product

$$\langle\phi|\phi'\rangle=\frac{2}{\pi}\int_{z=-\pi/2}^{z=\pi/2}\phi(z)\phi'(z)dz, \tag{C.1}$$

whose normalization has been chosen such that $\langle S_n|S_{n'}\rangle=\langle C_n|C_{n'}\rangle=\delta_{n,n'}$. All the scalar products can be easily calculated, so we do not give their values, but only choose the signs of the functions inside the scalar products such that they are all positive numbers. The series are truncated at a cutoff n_{max}; *e.g.* $\theta=\sum_{n=1}^{n_{max}}\theta_n(\mathbf{r})S_n(z)$. In practice, $n_{max}=4$ gives good numerical results, of an accuracy of $\simeq 0.1\%$ as compared to exact calculations with very high n_{max}, and is used for all our calculations except in Section 3. There $n_{max}=2$ is used to allow for analytic calculations; note that this is the minimal value of n_{max} because of the $z-$symmetry properties discussed in Section 2.2. The accuracy is then reduced to only a few %.

The full linear equations of the problem can be found in [8]. After projections of the n_y, n_z, f, g and θ equations on S_2, S_1, C_1, S_2 and S_1 respectively, one obtains for the linear modes (3.2) within the lowest-order Galerkin approximation:

$$\begin{aligned}F\sigma\tilde{n}_y &= -K_{yy}\,\tilde{n}_y + ip(k_{11}-k_{22})\,\langle S_2|S_1'\rangle\,\tilde{n}_z\\ &\quad - Fqp\,\langle S_2|C_1'\rangle\,\tilde{f}+Fq^2\tilde{g},\end{aligned} \tag{C.2}$$

$$\begin{aligned}F\sigma\tilde{n}_z &= -K_{zz}\,\tilde{n}_z + ip(k_{22}-k_{11})\,\langle S_1|-S_2'\rangle\,\tilde{n}_y\\ &\quad + Fiq\mathbf{q}^2\,\langle S_1|C_1\rangle\,\tilde{f},\end{aligned} \tag{C.3}$$

$$\begin{aligned}&Pr^{-1}\mathbf{q}^2(\mathbf{q}^2+\langle C_1|-C_1''\rangle)\sigma\tilde{f}\\ &\quad + iq(\alpha_3-\alpha_2\mathbf{q}^2)\,\langle C_1|S_1\rangle\,\sigma\tilde{n}_z+\gamma_2 qp\,\langle C_1|S_2'\rangle\,\sigma\tilde{n}_y\\ &= -\mathcal{V}_{ff}\,\tilde{f}+qp\,(\gamma_3(\mathbf{q}^2+4)-\alpha_1 q^2)\,\langle C_1|-S_2'\rangle\,\tilde{g}\\ &\quad + \mathbf{q}^2\,\langle C_1|S_1\rangle\,\tilde{\theta}\end{aligned} \tag{C.4}$$

$$\begin{aligned}&Pr^{-1}\mathbf{q}^2\sigma\tilde{g}+i\alpha_3 p\,\langle S_2|S_1'\rangle\,\sigma\tilde{n}_z+(\alpha_2 q^2-\alpha_3 p^2)\sigma\tilde{n}_y\\ &= -\mathcal{V}_{gg}\,\tilde{g}+qp\,(\gamma_3(\mathbf{q}^2+4)-\alpha_1 q^2)\,\langle C_1|-S_2'\rangle\,\tilde{f},\end{aligned} \tag{C.5}$$

$$\sigma\tilde{\theta}=-\mathcal{K}\,\tilde{\theta}+R\,\langle S_1|C_1\rangle\,\mathbf{q}^2\tilde{f}-R\kappa_a iq\tilde{n}_z, \tag{C.6}$$

with the constants defined in Section 3.1. For simplicity we have assumed here and in Section 3.1 that $\alpha_{32}=0$ in the director equations. This does not change the value of the linear threshold R_c (Sect. 3.2) by more than 1% for all the nematics mentioned in Appendix A.

References

1. See for instance P.-G. de Gennes, *The Physics of Liquid Crystals* (Clarendon Press, Oxford, 1993), and references therein.
2. For a recent review see A. Buka, L. Kramer, *Pattern formation in liquid crystals* (Springer-Verlag, New-York, 1996).
3. A. Joets, R. Ribotta, J. Phys. France **47**, 595 (1986).
4. S. Kai, W. Zimmermann, Prog. Theor. Phys. Sup. **99**, 458 (1989).
5. E. Guyon, P. Pieranski, C.R. Acad. Sci. **274**, 656 (1972); E. Dubois-Violette, E. Guyon, P. Pieranski, Mol. Cryst. Liq. Cryst. **26**, 193 (1974).
6. See L.I. Berge, G. Ahlers, D.S. Cannell, Phys. Rev. E **48**, R3236 (1993), and also the contribution of G. Ahlers in [2].
7. E. Dubois-Violette, C.R. Acad. Sci. **273**, 923 (1971); E. Dubois-Violette, Solid State Commun. **14**, 767 (1974).
8. Q. Feng, W. Pesch, L. Kramer, Phys. Rev. A **45**, 7242 (1992).
9. E. Plaut, R. Ribotta, Europhys. Lett. **38**, 441 (1997).
10. E. Plaut, L. Pastur, R. Ribotta, second part of this paper (experiments), Eur. Phys. J. B **5**, 283 (1998).
11. See M.C. Cross, P.C. Hohenberg, Rev. Mod. Phys. **65**, 851 (1993), or A.C. Newell, T. Passot, J. Lega, Annu. Rev. Fluid Mech. **25**, 399 (1993).
12. P. Manneville, *Dissipative Structures and weak Turbulence* (Academic Press, New York, 1990).
13. We use the hydrodynamic convention, which states that the force exerted on a surface element $\mathbf{dS}$ is $\mathbf{df} = \underline{\underline{\sigma}} \cdot \mathbf{dS}$. In [1] was used a different convention which transposes the stress tensor.
14. O. Parodi, J. Phys. France **31**, 581 (1970).
15. In [8] a formula analogous to (3.17) has been given, but it suffered from several misprint errors, and moreover the neutral modes were not explicited.
16. These values differ from the exact ones, obtained *e.g.* with high-order Galerkin expansion, $R_c^{iso} = 1708/\pi^4 = 17.53$, $q_c^{iso} = 3.1163/\pi = 0.9920$, less than 1.2%.
17. Additionally, we do not split in (4.11) the contributions of the couplings according to equation 4.5. If this would be done a much longer diagram would be obtained, which would be more complicated to interpret. Preferentially, the splitting should only be performed *a posteriori* for the important terms, if one wants to analyze them in details.
18. The contribution (N1) is proportional to $Fq\tilde{f}(\mathbf{q})\tilde{n}_z^2(\mathbf{q})$ up to some numerical constants, whereas the magnetic contribution quoted in [8] is proportional to $h^2\tilde{n}_z^3(\mathbf{q})$. The corresponding ratio $Fq/h^2\tilde{f}(\mathbf{q})/\tilde{n}_z(\mathbf{q})$ is typically large at intermediate h, since according to equation 3.13 the velocity modulation becomes larger with increasing h in comparison with the director distortion.
19. P. Coullet, C. Elphick, L. Gil, J. Lega, Phys. Rev. Lett. **59**, 884 (1987).
20. S. Ciliberto, P. Coullet, J. Lega, E. Pampaloni, C. Perez-Garcia, Phys. Rev. Lett. **65**, 2370 (1990).
21. R. Yang, F.K. Browand, P. Coullet, P. Huerre, J. Fluid Mech. **248**, 403 (1993).
22. E. Bodenchatz, W. Pesch, L. Kramer, Physica D **32**, 135 (1988).
23. See *e.g.* R. Ribotta, A. Joets, J. Phys. France **47**, 739 (1986).
24. A. Tschammer, W. Pesch, private communication.
25. The modes intervening in (7.1, 7.2) have to be calculated at such an ϵ value. For instance, using the neutral mode $V_1(\mathbf{k})$ at $\epsilon = \epsilon_0(\mathbf{k})$ for $\mathbf{k}$ far from $\mathbf{q}$, and performing the other calculations at $\epsilon = \epsilon_0(\mathbf{q})$, would be irrelevant, since $\epsilon_0(\mathbf{k})$ can get very large for $\mathbf{k}$ far from $\mathbf{q}$.
26. E. Plaut, R. Ribotta, Phys. Rev. E. **56**, R2375 (1997).
27. A.G. Rossberg, A. Hertrich, L. Kramer, W. Pesch, Phys. Rev. Lett. **76**, 4729 (1996).
28. E. Plaut, W. Decker, A. G. Rossberg, L. Kramer, W. Pesch, A. Belaidi, R. Ribotta, Phys. Rev. Lett. **79**, 2367 (1997).
29. H. Kneppe, F. Schneider, N.K. Sharma, Ber. Bunsenges. Phys. Chem. **85**, 784 (1981).
30. H. Kneppe, F. Schneider, N.K. Sharma, J. Chem. Phys. **77**, 3203 (1982).
31. R. Vilanove, E. Guyon, C. Mitescu, P. Pieranski, J. Phys. **35**, 153 (1974); W.H. de Jeu, W.A.P. Claassen, A.M. Spruijt, Mol. Cryst. Liq. Cryst. **37**, 269 (1976).
32. H.H. Graf, H. Kneppe, F. Schneider, Molec. Phys. **77**, 521 (1992).
33. E. Plaut, Ph.D. thesis, Université d'Orsay, 1996.
34. S. Chandrasekhar, *Hydrodynamic et Hydromagnetic Stability* (Clarendon Press, Oxford, 1968).